56p

NASA TECHNICAL NOTE

NASA TN D-2194

NASA TN D-2194

N64-22020

CODE-1 CAT. 32

THE ECHO I INFLATION SYSTEM

by Dewey L. Clemmons, Jr.

Langley Research Center
Langley Station, Hampton, Va.

NATIONAL AERONAUTICS AND SPACE ADMINISTRATION • WASHINGTON, D. C. • JUNE 1964

THE ECHO I INFLATION SYSTEM

By Dewey L. Clemmons, Jr.

Langley Research Center
Langley Station, Hampton, Va.

NATIONAL AERONAUTICS AND SPACE ADMINISTRATION

For sale by the Office of Technical Services, Department of Commerce,
Washington, D.C. 20230 -- Price $1.50

CONTENTS

	Page
SUMMARY	1
INTRODUCTION	1
SYMBOLS	3
DESCRIPTION OF SATELLITE	7
ENVIRONMENTAL CONDITIONS	11
Thermal Analysis	11
Orbital geometry	11
Space-environment heat transfer	13
Equilibrium temperature	16
Thermal response	19
Micrometeoroid Impact and Penetration	22
Deforming Loads	26
Static atmospheric pressure	26
Dynamic atmospheric pressure	26
Micrometeoroid pressure	27
Solar radiation pressure	28
Memory of folds	28
INFLATION MEDIUM	29
Considerations	29
Vapor Pressure of Compounds	33
Selecting the Compound	34
Quantity of Compound	36
Pressure Time History	37
Mass Flow Rate	40
ORBITAL RESULTS AND DISCUSSION	41
CONCLUDING REMARKS	42
APPENDIX A - THERMAL RESPONSE OF A SPHERICAL SATELLITE ENTERING AND LEAVING SHADOW OF EARTH	44
APPENDIX B - CALCULATION OF PRESSURE TIME HISTORY INSIDE A VESSEL	48
REFERENCES	50
TABLES	52

THE ECHO I INFLATION SYSTEM

By Dewey L. Clemmons, Jr.

SUMMARY

22020

A study has been made to determine the feasibility and selection of a subliming compound to be used as an inflation system for the Echo I satellite. Primary considerations have been given to the compatibility of such a system with payload weight limitations, storage in satellite, internal pressure requirements, and the minimum length of time that the inflation need be sustained. Calculations are made to determine the temperature variations of the satellite while in sunlight and shadow, the deforming loads present in the environment of space, the effects of micrometeoroids with regard to holes punctured in the satellite, the method of selecting the proper subliming compound as well as the pressure time history and mass flow rate of the inflation vapors.

It can be generalized from this investigation that subliming organic compounds lend themselves very well to the initial inflation of large, thin wall, spherical configurations in orbit above the earth's atmosphere and pressure sustenance can be achieved for periods of the order of a few weeks. In particular, it was found for the Echo I satellite that (1) the thermal response would be so rapid that a continuous sunlight orbit would be required for the subliming compound to achieve maximum performance, (2) the maximum deforming loads would result from the satellite's memory of its original folded configuration, (3) micrometeoroid hole area would be produced at the rate of about 28.1 square centimeters per day, and (4) the inflation and pressure sustenance requirement would be satisfied with 4.54 kilograms of benzoic acid and 9.18 kilograms of anthraquinone to maintain a pressure of about 10^{-3} torr for about 13 days for evaluation of the satellite as a passive communications relay station.

A comparison between the predicted performance of the inflation system and that inferred by experimental scattering of microwave signals by the satellite is discussed. The referenced experimental evidence indicates that the sphericity of the satellite began to degrade after a period of 6 to 12 days after launch.

AUTHOR

INTRODUCTION

The Echo I satellite was designed as an experimental, spherical, passive radio relay station to be placed in a circular orbit around the earth for the purpose of evaluation as a means of increasing worldwide communications. The advantages of such a satellite are that it permits the extension of the usable radio-frequency spectrum for long-range communications between points on the

earth, as well as providing continuous surface coverage over the range of mutual visibility for transmitting and receiving stations. The frequency spectrum is extended by reflecting signals back to the earth that are of sufficiently high frequency to penetrate the ionosphere. The surface coverage is increased by virtue of the fact that the spherical reflector is an isotropic scatterer of electromagnetic radiation that will permit signal reception at all points on the earth's surface that are geometrically visible from the satellite. This is an improvement over the method of radio communication over long ranges by reflecting signals off the ionosphere where large voids remain in surface coverage between the points where the signal is reflected from the earth and ionosphere.

The spherical shape of the satellite is advantageous for a number of reasons: (1) its spherical symmetry eliminates the need for any orientation control, (2) it permits the development of high stresses in the skin by an inflation gas without the occurrence of stress concentrations that would have to be reinforced by weight penalizing materials, and (3) the previously mentioned isotropic scattering characteristic that affords equal opportunity for all stations to use the satellite as long as it remains mutually visible to sender and receiver. Since the satellite acts as a passive relay station, it has the capability of reflecting all frequencies simultaneously and eliminating frequency channel restrictions that would be imposed by an active repeater.

It was determined that a satellite 30.48 meters (100 feet) in diameter would be compatible with presently existing research transmitting facilities in relaying voice communications over the range involved while maintaining sufficient signal strength to be received at the receiving stations. The large sphere was designed to be placed in a circular orbit 1668 kilometers above the earth's surface. In keeping with the payload weight and size limitations imposed by the launching vehicle, it was required that the folded sphere and its inflation system weigh only 68 kilograms and fit inside a spherical container only 67 centimeters in diameter. The inflation compounds weighed 13.6 kilograms. Once the payload was injected into orbit, it was programed to be separated from the last-stage spent rocket motor by a spring-loaded mechanism. After a sufficient time had elapsed for a separation distance of approximately 60 meters to exist between the rocket motor and payload container, the two container hemispheres were accelerated away from each other by means of an explosive charge.

While conforming with the weight requirements, the inflation system was required to erect the folded configuration to a spherical shape and stress the skin so that no irregularities would remain that would distort the incident radio signals and maintain a minimum internal pressure for the 1- to 2-week test period necessary to evaluate the satellite as a passive radio relay station.

Before this experiment there had never been an attempt to erect such a large, thin-wall structure in space. In the past, conventional methods utilizing bottled, compressed gas had been satisfactory for smaller, thicker walled, inflatable satellites where weight and storage of necessary quantities were not of prime consideration. In this application consideration was given

to several aspects of the gas bottle method which included: (1) the weight of the bottles required to store sufficient quantities of gas to erect and sustain the pressure during the test period, (2) the complications arising from attempts to store the bottle with the compactly folded satellite, (3) the danger of the gas leaking from the bottles during payload storage and transit that would cause the satellite to virtually explode when released in the vacuum of space and, (4) the complications involved in a method to actuate gas injection into the satellite at the proper time and at the proper rate. The obvious problems associated with these considerations leave a great deal to be desired in this method of inflation. A novel concept conceived for the Echo I inflation was based on the principle of subliming compounds that could be distributed throughout the inside of the sphere in a loose powder form in such a manner that it lends itself to the folding and packaging technique. The powders must be of such character that they can be induced to liberate vapors for erecting and maintaining inflation once the satellite is in orbit.

The purpose of this paper is to present an analysis of the factors affecting the erection and pressure sustenance of the Echo I satellite by using the sublimation principle and to show, from this analysis, a method of selecting subliming compounds that will meet the requirements previously stated. Details are presented with regard to the dynamic thermal response of the satellite, deforming loads, effects of micrometeoroids, selection of subliming compounds, pressure time history inside the satellite, and the rate of mass flow of vapors out of the satellite as a result of leakage.

SYMBOLS

A	area, cm^2
A'	thermodynamic constant, dimensionless
a	earth's albedo, assumed 0.36
B'	thermodynamic constant, $^{o}K^{-1}$
C'	a simplifying collection of terms, $3.64 \times 10^3 \sqrt{\frac{T}{MV^2}}$, cm^{-2}-sec^{-1}
C_S	solar radiation constant, 1.3953×10^6 ergs-sec^{-1}-cm^{-2}
c	velocity of light in vacuo, 2.99776×10^{10} cm-sec^{-1}
c'	constant of integration, dynes-cm^{-2}
c_p	specific heat of the form $y^2 + z^2T$, erg-gm^{-1}-$^{o}K^{-1}$
D	diameter, cm

d	depth of penetration, cm
dm/dt	mass flow rate, gm-sec^{-1}
dq/dt	heat flow rate, erg-sec^{-1}
$d\bar{T}/dt$	average temperature change rate, ^{o}K-sec^{-1}
E	modulus of elasticity, dynes-cm^{-2}
F_R	geometric view factor, dimensionless
f	air orifice hole size, cm^2
g	rate of micrometeoroid hole growth, cm^2-sec^{-1}
g_o	gravitational acceleration at earth's surface, 9.814×10^2 cm-sec^{-2}
h	satellite altitude, cm
I	influx, micrometeoroids-sec^{-1}
j	ratio of microscopic surface to apparent surface area, dimensionless
E_k	kinetic energy, ergs
k	$\frac{R_E}{R_E + h}$, dimensionless
k'	Boltzmann's constant, 1.3803×10^{-16} ergs-molecule^{-1}-^{o}K^{-1}
M	molecular weight, gm-(gm-mole)$^{-1}$
m	mass, gm
N	number of molecules, molecules
N_g	Avogadro's number, 6.025×10^{23} molecules-(gm-mole)$^{-1}$
n	number molecular density, molecules-cm^{-3}
p	pressure, dynes-cm^{-2}
q	thermal energy, ergs
R	radius, cm
R_g	universal gas constant, 8.3149×10^7 ergs-(gm-mole)$^{-1}$-^{o}K^{-1}

S	skin stress, dynes-cm^{-2}
T	absolute temperature, ^{o}K
$\bar{T}$	absolute temperature averaged over surface, ^{o}K
t	time, sec
t'	thickness, cm
u	visual magnitude, dimensionless
V	volume, cm^3
v	velocity, cm-sec^{-1}
W	weight, gm
w	a simplifying collection of terms, $\sqrt{\frac{\pi R_B^2 C_S \alpha_E}{m}\left(\frac{1-a}{2}\right)\left[1-\left(1-k^2\right)^{1/2}\right]}$, ergs$^{1/2}$-gm$^{-1/2}$-sec$^{-1/2}$
w_1	a simplifying collection of terms, $\sqrt{\frac{\pi R_B^2 C_S \alpha_S}{m}\left\{1+\left(2aF_R+\frac{\alpha_E}{\alpha_S}\frac{1-a}{2}\right)\left[1-\left(1-k^2\right)^{1/2}\right]\right\}}$, ergs$^{1/2}$-gm$^{-1/2}$-sec$^{-1/2}$
X,Y,Z	Cartesian coordinate axes
x	a simplifying collection of factors, $\sqrt{\frac{4\pi R_B^2 \epsilon_o \sigma}{m}}$, ergs$^{1/2}$-gm$^{-1/2}$-sec$^{-1/2}$
y,z	specific heat constants used in defining c_p
α	total absorptance to thermal radiation, dimensionless
β	displacement between satellite position and earth-sun line, deg
γ	displacement between satellite position and nearest approach to sun, deg
δ	angle between orbital plane normal and earth-sun line, deg
ϵ	total hemispherical emittance, dimensionless
ζ	heat to vaporization, ergs-gm^{-1}
λ	latent heat of sublimation, ergs-(gm-mole)$^{-1}$

ν	Poisson's ratio, dimensionless
ρ	atmospheric density, gm-cm^{-3}
ρ'	density of film, gm-cm^{-3}
σ	Stefan-Boltzmann radiation constant, 5.71×10^{-5} ergs-cm^{-2}-sec^{-1}-^{o}K^{-4}

Subscripts:

a	anthraquinone
B	satellite
b	benzoic acid
C	coldspot
cr	critical
E	earth
H	hotspot
i	inside surface
n	normal
o	outside surface, initial time
R	reflected from earth
S	solar
sh	in shadow
su	in sunlight
T	thermal
u	visual magnitude
V	vapor

Conversion Factors:

1 kilometer = 0.5396 nautical miles

1 meter = 3.281 feet

1 centimeter = 0.3937 inch

1 square meter = 10.76 square feet

1 square centimeter = 0.1550 square inch

1 torr = 1.0000 millimeter of mercury pressure

1 dyne per square centimeter = 1.450×10^{-5} pounds per square inch

1 dyne per square centimeter = 7.5×10^{-4} torr

1 kilogram = 2.205 pounds

1 erg = 2.389×10^{-8} gm-calorie

DESCRIPTION OF SATELLITE

The Echo I satellite was constructed from 0.00127-centimeter (0.5 mil) thick poly [ethylene terephthalate] plastic film with approximately 2,200 angstroms of aluminum vapor deposited on the outside surface. The thin film of aluminum serves two purposes: first, it reflects the incident communication signals, having a reflectivity greater than 97 percent in the 400- to 10,000-megacycle range (ref. 1), and second, it protects the film from damaging ultraviolet radiation (ref. 2).

The aluminum was vapor deposited on long rolls of 137.16-centimeter-wide plastic film. From these rolls, 82 gores required for the construction of each inflatable sphere were cut into the required shape, sealed together with splice-plate tape, and capped at each polar end. (See fig. 1.) The gores are

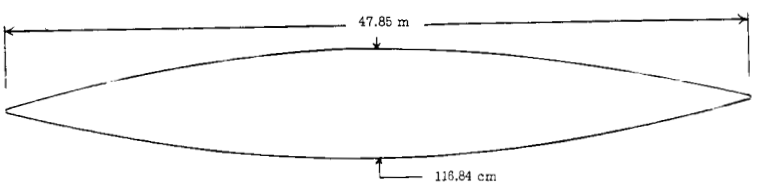

(a) Gore.

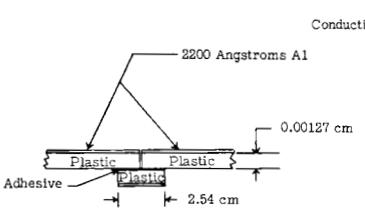

(b) Gore seam.

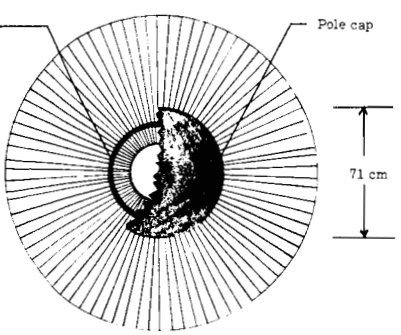

(c) Polar end construction.

Figure 1.- Fabrication of the Echo I satellite.

approximately 116.84 centimeters wide at the equator and 47.85 meters long as seen in figure 1(a). These gores were butted together and sealed with a 2.54-centimeter-wide tape made from the same material as used for the gores with a thin layer of thermosetting resin applied to the plastic side of the film to serve as the adhesive. (See fig. 1(b).) The tape was applied to the inside surface of the sphere. The polar end construction was made by first placing a conducting ring of paint around the pole and then sealing a polar cap 71 centimeters in diameter over the conducting ring and gore terminations. (See fig. 1(c).) The conducting ring was placed around the polar end to electrically connect all the gores together, which are otherwise insulated by the plastic film dielectric along the gore seams. This procedure is a precautionary measure taken to enhance the isotropic scattering characteristics of the sphere by decreasing the possibility that the insulated gores might act as radiating dipoles.

A full-scale sphere, 30.48 meters in diameter, weighing only 54.42 kilograms is seen inflated in figure 2. The striped pylons on either side of the sphere are 3.048 meters high to serve as reference scales in the figure. The unusual pattern of images on the sphere is reflected from the building walls.

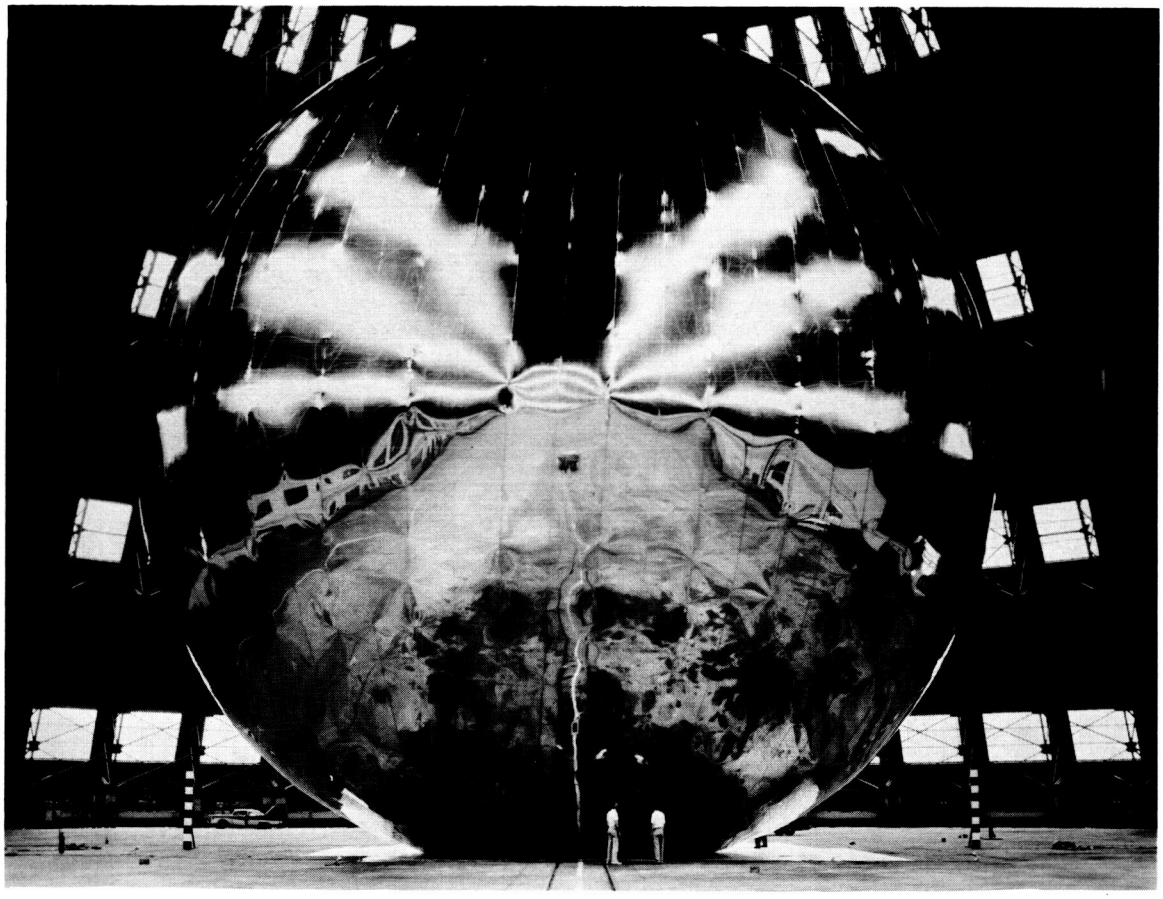

Figure 2.- Fully inflated 30.48-meters-diameter Echo I. L-58-3473

In preparation for flight, the large sphere is folded and packaged inside a 67.31-centimeter-diameter container made of magnesium alloy. Figure 3 shows

Figure 3.- Full-scale plastic canister model with 30.48-meter-diameter Echo I packed inside. L-59-3364

it packaged inside a plastic model of the container. The linear shaped charge used to cut the lacing cords and accelerate the two container halves apart after it is launched into orbit and separated from the vehicle can be seen lying along the equator of the container between the two flanges. The cable seen passing from the container base to the equator carries power from a set of small nickel-cadmium batteries to the initiator for firing the shaped charge.

The actual container with inflatable sphere packaged inside is seen in figure 4. It is mounted on top of the rocket motor from which it was separated

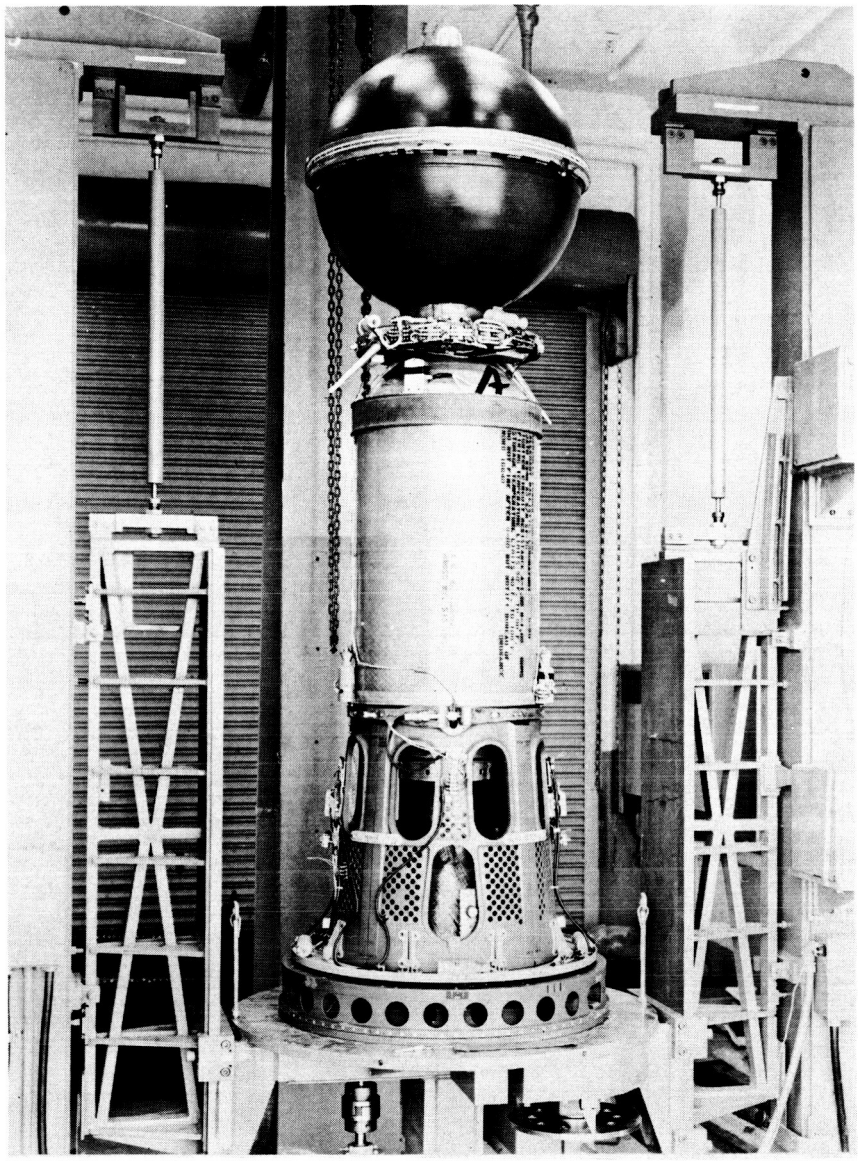

Figure 4.- Echo I payload mounted at top of third-stage Thor-Delta launch vehicle. L-59-7527

by a spring-loaded mechanism after injection into orbit. The rocket motor is the third stage of the three-stage Thor-Delta launch vehicle. After about 60 meters separation distance between the spent rocket motor and the canister had been attained, the canister halves were separated by the shaped charge, and the satellite was free to inflate. The subsequent part of this report will include some environmental conditions of the orbit and the satellite inflation technique.

ENVIRONMENTAL CONDITIONS

Thermal Analysis

The Echo I satellite has the smallest ratio of mass to frontal area of any satellite ever placed in orbit around the earth by man. The basic structure, excluding the inflation compound, weighs only 54.42 kilograms and has an external surface area of 2,952 square meters. This characteristic results in very fast thermal response of the satellite as it passes through the varying thermal environment of space. It is shown herein that for all practical purposes, the satellite remains in thermal equilibrium with its environment while in the sunlight portion of its orbit; thus, its temperature is almost independent of time and is only a function of position. It is also shown that even though the thermal response in the shadow is not as rapid as in the sunlight, it is still so rapid that the satellite can be allowed virtually no time in the shadow if the subliming inflation system is to be continuously effective during the test period.

Orbital geometry.- The satellite's position in a circular orbit above the earth's surface can be described by three parameters, $R_E + h$, γ, and δ, as seen in figure 5. This geometric model was selected for simplicity since the

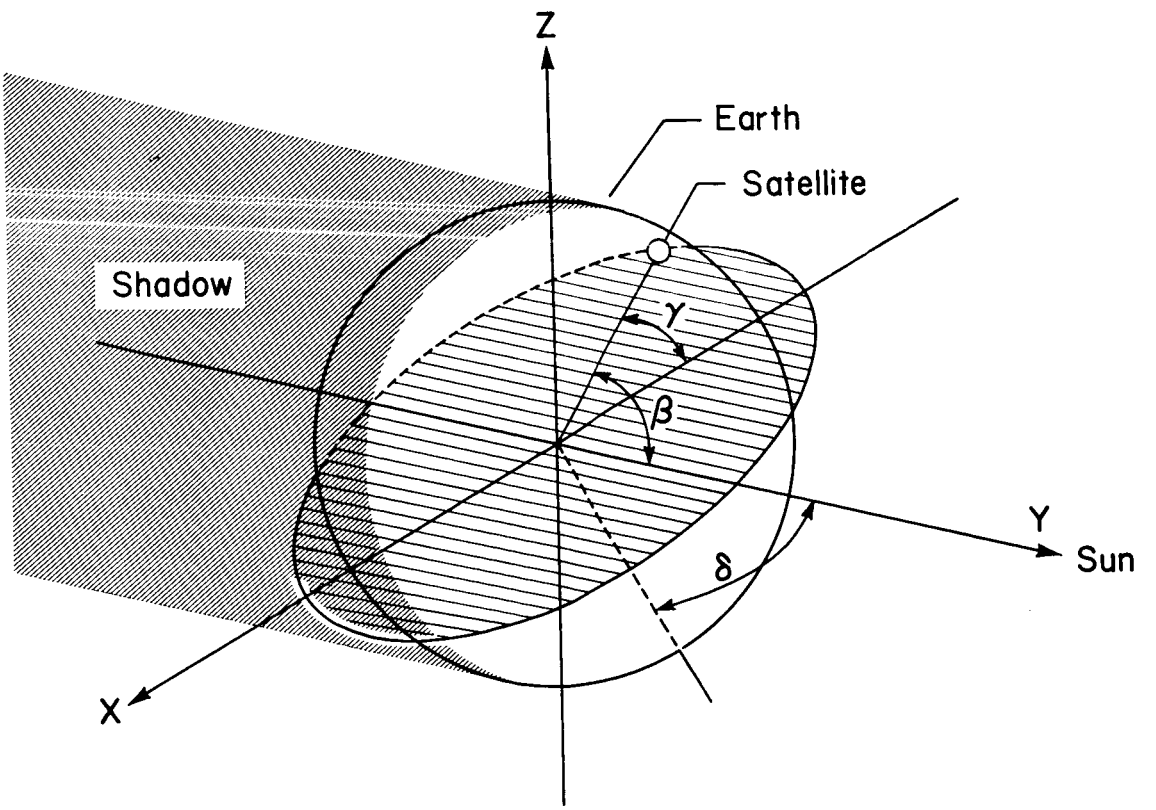

Figure 5.- Circular orbit geometry.

thermal energy present in the space environment is distributed symmetrically about the earth-sun line. The angle γ describes the displacement of the orbital radius vector from the nearest approach of the satellite to the sun and is limited to $0 \leqq \gamma \leqq 2\pi$, measured in the plane of the orbit. The displacement of the normal to the orbital plane from the earth-sun line is described by δ and is limited to $0 \leqq \delta \leqq \pi/2$. The Cartesian coordinates of the satellite position can be written as

$$X = \left(R_E + h\right)\sin \gamma \tag{1}$$

$$Y = \left(R_E + h\right)\cos \gamma \sin \delta \tag{2}$$

$$Z = \left(R_E + h\right)\cos \gamma \cos \delta \tag{3}$$

The satellite will enter the earth's shadow during each orbital period when $\delta > \cos^{-1}k$ and $\frac{\pi}{2} \leqq \gamma \leqq \frac{3}{2}\pi$. The angle γ of entry and exit can be determined as a function of δ by substitution of equations (1) and (3) into the equation of the circle encompassing the earth's shadow concentric with the Y-axis

$$X^2 + Z^2 = R_E^2 \tag{4}$$

Substitution of equations (1) and (3) into equation (4) and simplification gives

$$\gamma = \sin^{-1}\left(\pm\sqrt{\frac{k^2 - \cos^2\delta}{\sin^2\delta}}\right) \qquad \left(\cos \delta \leqq k\right) \tag{5}$$

It is also necessary to know the displacement of the radius vector of the satellite position from the earth-sun vector described in figure 5 by β, where this angle is limited to $0 \leqq \beta \leqq \pi$. The amount of earth-reflected solar radiation incident on the satellite depends on this angle. It can be shown by projecting the satellite position onto the Y-axis that

$$\cos \beta = \cos \gamma \sin \delta \tag{6}$$

Figure 6 contains graphical relations between β and γ for various orbital plane inclinations δ, as determined from equation (6). Solutions of equation (5) have also been superimposed on this figure which shows the portions of each orbit that pass through the earth's shadow for circular orbit altitudes of 927, 1668, and 2780 kilometers. It can be seen, for example, that when $\delta = 40^\circ$, the satellite would remain in continuous sunlight if in a 2780-kilometer orbit,

in the shadow for $161.6 \leqq \gamma \leqq 198.4$ if in a 1668-kilometer orbit, and in the shadow for $139.4 \leqq \gamma \leqq 220.6$ if in a 927-kilometer orbit.

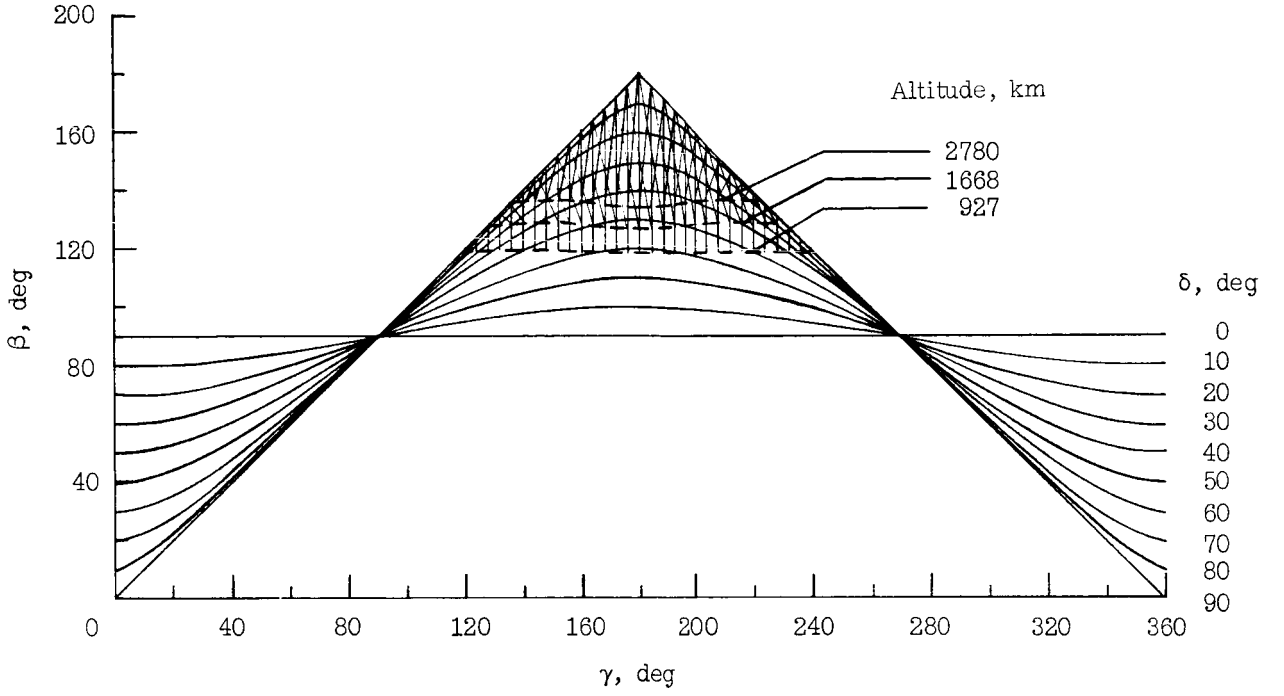

Figure 6.- Relation between satellite position parameters and earth's shadow for circular orbit altitudes of 927, 1668, and 2780 kilometers.

Space-environment heat transfer.- The heat transfer to the satellite is considered to be entirely radiative since the circular orbit is at an altitude of 1668 kilometers where aerodynamic heat transfer can be neglected. The three sources of heat input are: (1) direct radiation from the sun, (2) reflected solar radiation from the earth, and (3) direct radiation from the earth. The general differential equation of heat transfer for the satellite is

$$\left(\frac{dq}{dt}\right)_S + \left(\frac{dq}{dt}\right)_R + \left(\frac{dq}{dt}\right)_E - \left(\frac{dq}{dt}\right)_B = mc_p \frac{d\overline{T}}{dt} \tag{7}$$

Expressions for the first three terms in equation (7), which are the absorption rates of the direct solar radiation, solar radiation reflected from the earth, and direct radiation from the earth, respectively, are derived in reference 2 as

$$\left(\frac{dq}{dt}\right)_S = \pi R_B{}^2 C_S \alpha_S \tag{8}$$

$$\left(\frac{dq}{dt}\right)_R = \pi R_B{}^2 C_S \alpha_S a 2\left[1 - \left(1 - k^2\right)^{1/2}\right] \tag{9}$$

$$\left(\frac{dq}{dt}\right)_E = \pi R_B{}^2 C_S \alpha_E \frac{1 - a}{2}\left[1 - \left(1 - k^2\right)^{1/2}\right] \tag{10}$$

The fourth term, which is the thermal radiation output of the satellite, can be expressed as

$$\left(\frac{dq}{dt}\right)_B = 4\pi R_B{}^2 \epsilon_o \sigma \overline{T}^4 \tag{11}$$

Equation (9) was derived for the special condition when the satellite is directly between the earth and the sun, $\beta = 0$. As the satellite moves from this position, the amount of radiation received decreases with increasing β until the shadow is reached where it is zero. The relation between the amount of earth-reflected radiation incident on a spherical satellite at a given altitude for various angles of β has been determined in reference 3. In figure 7

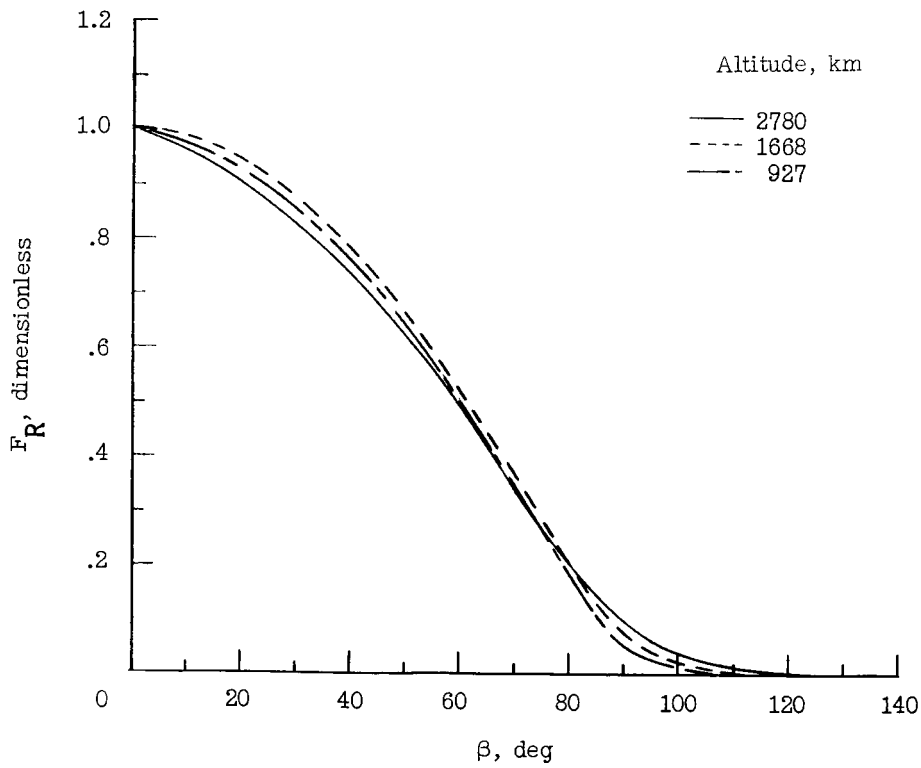

Figure 7.- The variation of incident earth reflected radiation on a satellite relative to the maximum amount received from this component when β is zero at altitudes of 927, 1668, and 2780 kilometers.

this relation can be seen for 927-, 1668-, and 2780-kilometer circular orbits. The geometric view factor $F_R(\beta)$ which is defined herein as the ratio of earth-reflected energy incident on the satellite relative to the amount incident when $\beta = 0$ is shown along the ordinate. It can be seen that $F_R(\beta)$ decreases rather rapidly until β reaches about 80° and then gradually decreases to zero at points where the satellite enters the shadow. Multiplying equation (9) by $F_R(\beta)$ will provide the magnitude of energy inputs from this source for any angle β.

The relative magnitude of thermal energy incident on a spherical satellite is shown in figure 8 for a 1668-kilometer orbit. It is easily seen that the direct solar radiation will be zero while the satellite is in the earth's shadow and remain at a constant level as long as it is in sunlight, the small variation in earth-sun distance being neglected. When β is less than $180^\circ - \cos^{-1}k$, the satellite will be in the sunlight, and when β is greater

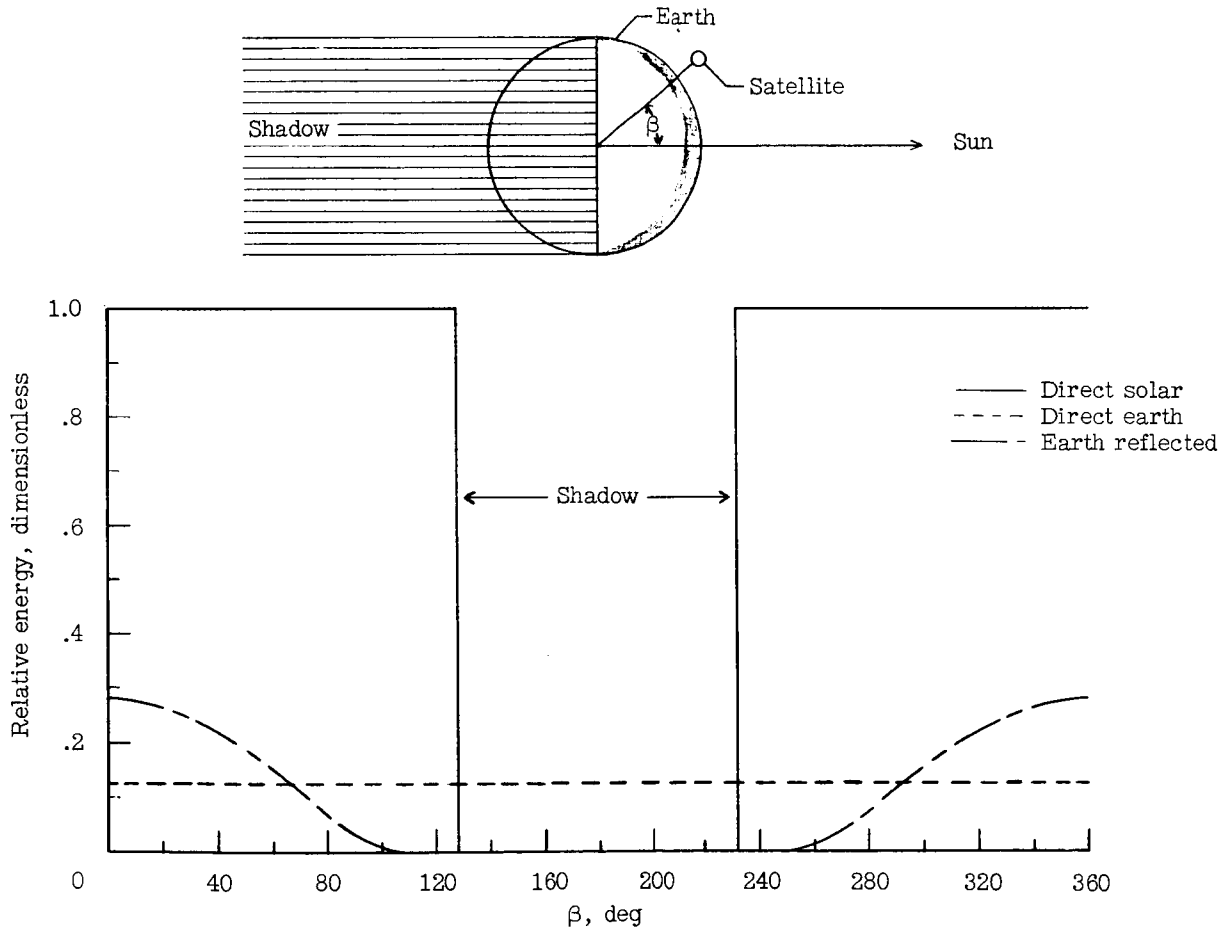

Figure 8.- Relative magnitude of radiant energy incident on a spherical satellite orbiting around the earth at an altitude of 1668 kilometers from direct solar, direct earth, and earth reflected solar radiation.

than $180^{\circ} - \cos^{-1}k$, it will be in the shadow. The direct radiation from the earth will remain constant regardless of the satellite position, any variation in thermal emission over the earth's surface being neglected. The relative energy incident from the earth-reflected component is seen to vary from a maximum of 28 percent when the satellite is directly between the earth and sun to 0 when the satellite enters the shadow.

Equilibrium temperature.- There are three different equilibrium temperatures of interest herein: (1) the fourth root of the average fourth-power temperature $\left(\text{that is, } \sqrt[4]{\overline{T^4}} = \overline{T}\right)$ distributed over the surface of the sphere, first while in the sunlight, and second, while in the earth's shadow; (2) the coldest spot T_C on the balloon during equilibrium in the sunlight; and (3) the hottest spot T_H on the balloon during equilibrium in the sunlight.

The fourth root of the average fourth-power temperature $\overline{T}$ of the satellite while in the sunlight can be determined by substituting equations (8) to (11) into equation (7), where equation (9) has been multiplied by the view factor $F_R(\beta)$. Setting the right-hand side equal to zero gives

$$\overline{T}_{su} = \sqrt[4]{\frac{C_S\alpha_S}{4\epsilon_o\sigma}\left\{1 + 2\left[aF_R(\beta) + \frac{1 - a}{4}\frac{\epsilon_o}{\alpha_S}\right]\left[1 - \left(1 - k^2\right)^{1/2}\right]\right\}} \tag{12}$$

The equilibrium temperatures predicted by this equation for a 1668-kilometer circular orbit appear in figure 9. The temperatures are plotted as a function

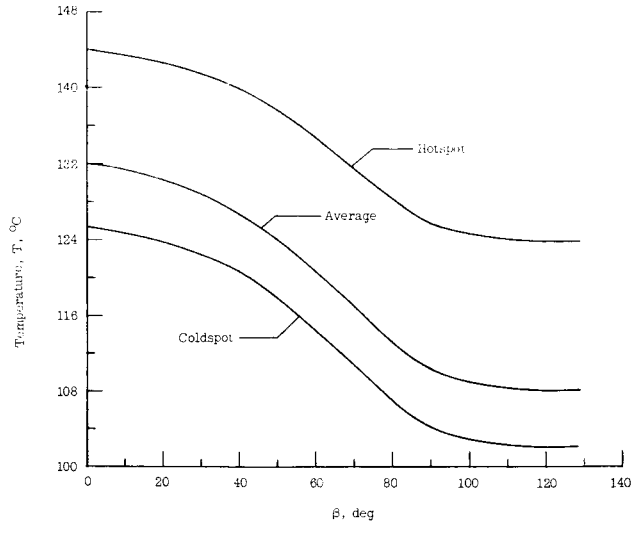

Figure 9.- Predicted variation of the equilibrium, hotspot, average, and coldspot temperature of Echo I while in the sunlight at an altitude of 1668 kilometers.

of β, where β is related to F_R, as seen in figure 7. The temperature is seen to vary over the range of 108° C to 132° C. This variation is attributed entirely to the variation of the earth-reflected component of radiation since the direct solar and direct earth components are constant during sunlight conditions.

The coldest spot on the balloon will occur in an area where heat input is smallest and will be in an area of the surface that can neither "see" the earth nor the sun. The heat transfer to and from this coldspot is assumed to be entirely radiative since the material is so thin that conduction can be neglected. The heat radiated away from the coldspot surface can be written as

$$\text{Heat out} = (\epsilon_i + \epsilon_o)\sigma T_{C,su}^{4} \tag{13}$$

since the shell is so thin that no appreciable temperature gradient can exist between the inside and outside surface. The heat input will come entirely from the inside of the satellite (because the outside surface is "looking" at the cold environment of space) and can be written as

$$\text{Heat in} = \epsilon_i \sigma \overline{T}_{su}^{4} \tag{14}$$

which is the quantity of heat received by all surface elements inside the spherical shell because of the internal radiative heat transfer (ref. 2). By setting equation (13) equal to equation (14), the coldspot temperature can be calculated with respect to the average temperature to give

$$T_{C,su} = \left(\frac{1}{1 + \frac{\epsilon_o}{\epsilon_i}}\right)^{1/4} \overline{T}_{su} \tag{15}$$

The hottest spot on the satellite will occur at a point where the sun's rays are normal to the surface since at this point the heat input is greatest. If only radiative heat transfer to and from this element of shell is considered, the heat output can be expressed as

$$\text{Heat out} = (\epsilon_i + \epsilon_o)\sigma T_{H,su}^{4} \tag{16}$$

The heat input at equilibrium can be expressed as

$$\text{Heat in} = \epsilon_i \sigma \overline{T}_{su}^{4} + \alpha_S C_S \tag{17}$$

where the first term describes the heat input to the inside surface and $\alpha_S C_S$ describes the input on the outside from direct solar radiation. By setting equation (16) equal to equation (17), the hotspot temperature can be calculated with respect to the average temperature as

$$T_{H,su} = \sqrt[4]{\left(\frac{\alpha_S}{\epsilon_i + \epsilon_o}\right)\frac{C_S}{\sigma} + \left(\frac{1}{1 + \frac{\epsilon_o}{\epsilon_i}}\right)\bar{T}_{su}^{\,4}} \tag{18}$$

The hotspot and coldspot temperatures corresponding to the average satellite temperature $\bar{T}$ while in the sunlight are shown in figure 9 for Echo I where $\epsilon_o = 0.03$, $\epsilon_i = 0.45$, and $\alpha_S = 0.10$. It is important to know the coldspot temperature since this temperature must be considered as the operating temperature when determining vapor pressure produced by a subliming compound used for inflation. (The coldspot can be as large as one-eighth the total satellite surface.) The hotspot is required in evaluating adhesives for sealing the satellite gores together under conditions of maximum temperature and internal-pressure-developed skin loading as well as other structural considerations. It can be seen from equation (12) that the variable parameter affording major control of the average satellite temperature $\bar{T}$ is α_S/ϵ_o while the temperature variation over the surface of the satellite can be minimized by making ϵ_o/ϵ_i as small as possible, as can be seen from equations (15) and (18). The relations among these three temperatures over a wide range of altitudes can be seen in figure 10. For example, at 927 kilometers the average

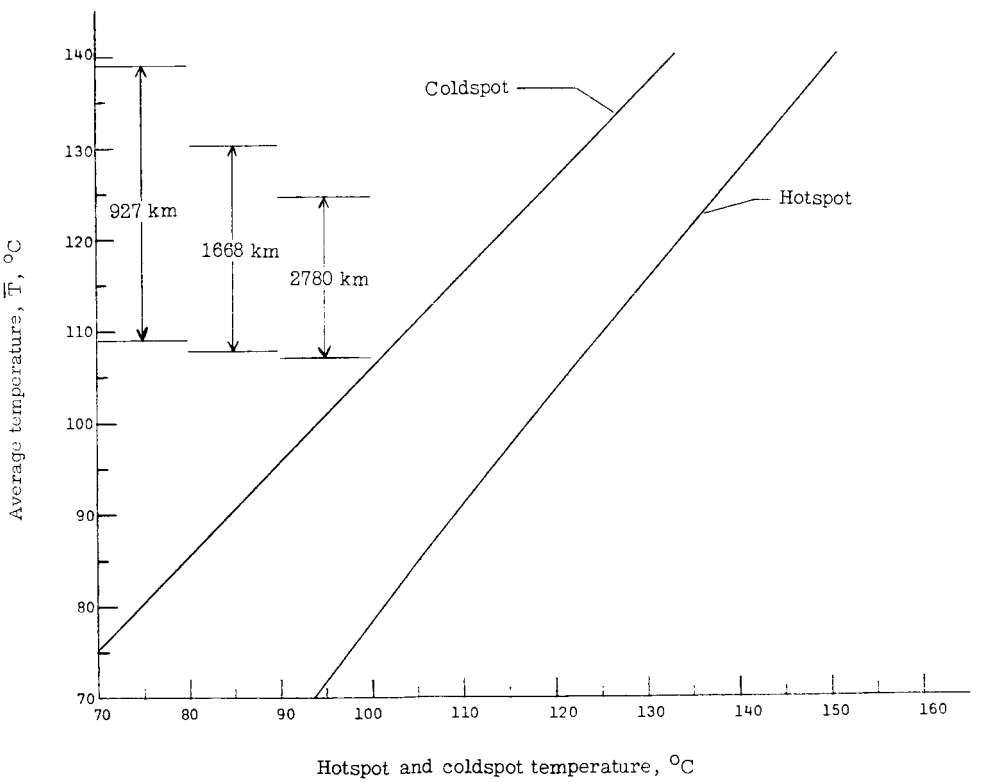

Figure 10.- Predicted variation of the Echo I hotspot and coldspot temperature with satellite average temperature. Average satellite temperatures possible while in the sunlight at three circular orbit altitudes are included.

temperature in the sunlight varies over the range 109° C to 139° C while the coldspot varies from 103° C to 132° C and the hotspot from 125° C to 150° C. It will be noticed that the minimum coldspot temperature on the satellite while in sunlight is affected only slightly with rather wide ranges of altitude, while the maximum hotspot is affected to a greater extent.

The equilibrium temperature of the satellite while in the shadow of the earth is determined by making the appropriate substitutions into equation (7), where the first two terms are now zero. The resulting equation is

$$\overline{T}_{sh} = \sqrt[4]{\frac{C_S \alpha_E}{4\epsilon_o \sigma} \frac{1 - a}{2} \left[1 - (1 - k^2)^{1/2}\right]} \tag{19}$$

A solution of this equation shows that the equilibrium temperature of a spherical satellite in the earth's shadow at an altitude of 1668 kilometers is -107° C. It is noted from this equation that the average equilibrium temperature in the shadow is independent of the thermal radiation characteristics of the satellite's surface when α_E is assumed equal to ϵ_o. This assumption can be made as a first approximation since the thermal radiation wavelength of both the earth and the satellite are of the same order of magnitude.

Thermal response.- The equilibrium temperature analysis presented above is indicative of the satellite temperature only if the satellite remains in the particular environment for a period of time sufficient for thermal equilibrium to be established. To predict the satellite temperature over a complete orbit, it is necessary to calculate the dynamic thermal response as it passes from one environment to the next. In the sunlight, the thermal environment changes as a result of variations in the earth-reflected radiation input. As the shadow is entered, the environment changes abruptly as the solar radiation is completely cut off. Equations for determining the dynamic thermal response of the satellite as it enters and exits the earth's shadow are derived in appendix A. The first case considered is that of entering the earth's shadow and is expressed as

$$t_{sh} = \frac{y^2}{2wx\sqrt{\frac{w}{x}}}\left(\tan^{-1}\frac{\overline{T}}{\sqrt{\frac{w}{x}}} - \frac{1}{2}\log_e \frac{\overline{T} - \sqrt{\frac{w}{x}}}{\overline{T} + \sqrt{\frac{w}{x}}}\right)\Bigg]_{\overline{T}_o}^{\overline{T}} - \frac{z^2}{4wx}\left(\log_e \frac{\overline{T}^2 - \frac{w}{x}}{\overline{T}^2 + \frac{w}{x}}\right)\Bigg]_{\overline{T}_o}^{\overline{T}} \tag{20}$$

The temperature decrease as a function of time predicted by this equation is seen in figure 11 where the specific heat of film was taken as $-1.14 \times 10^{-2} + 9.35 \times 10^{-4}\overline{T}$. The average satellite temperature was assumed to be 108° C as the shadow was entered. (See fig. 9.) A study of equation (20) shows that the rate at which the satellite cools is not independent of the surface characteristics as was the case for thermal equilibrium in the shadow. The higher, the emittance, the faster it will cool. Echo I, however, has a very low outside emittance (0.03), yet rapid cooling is evident. This property, of course, is due to its very low ratio of mass to area.

The second case considered is that of leaving the low-temperature environment of the earth's shadow and entering the sunlight. The equation for expressing the thermal response for this case is

$$t_{su} = \frac{y^2}{2w_1x\sqrt{\frac{w_1}{x}}}\left(\tan^{-1}\frac{\overline{T}}{\sqrt{\frac{w_1}{x}}} + \frac{1}{2}\log_e\frac{\sqrt{\frac{w_1}{x}} + \overline{T}}{\sqrt{\frac{w_1}{x}} - \overline{T}}\right)\Bigg]_{\overline{T}_o}^{\overline{T}} + \frac{z^2}{4w_1x}\left(\log_e\frac{\frac{w_1}{x} + \overline{T}^2}{\frac{w_1}{x} - \overline{T}^2}\right)\Bigg]_{\overline{T}_o}^{\overline{T}} \tag{21}$$

The temperature increase as a function of time predicted by this equation is also plotted in figure 11. It will be noticed that the initial temperature for

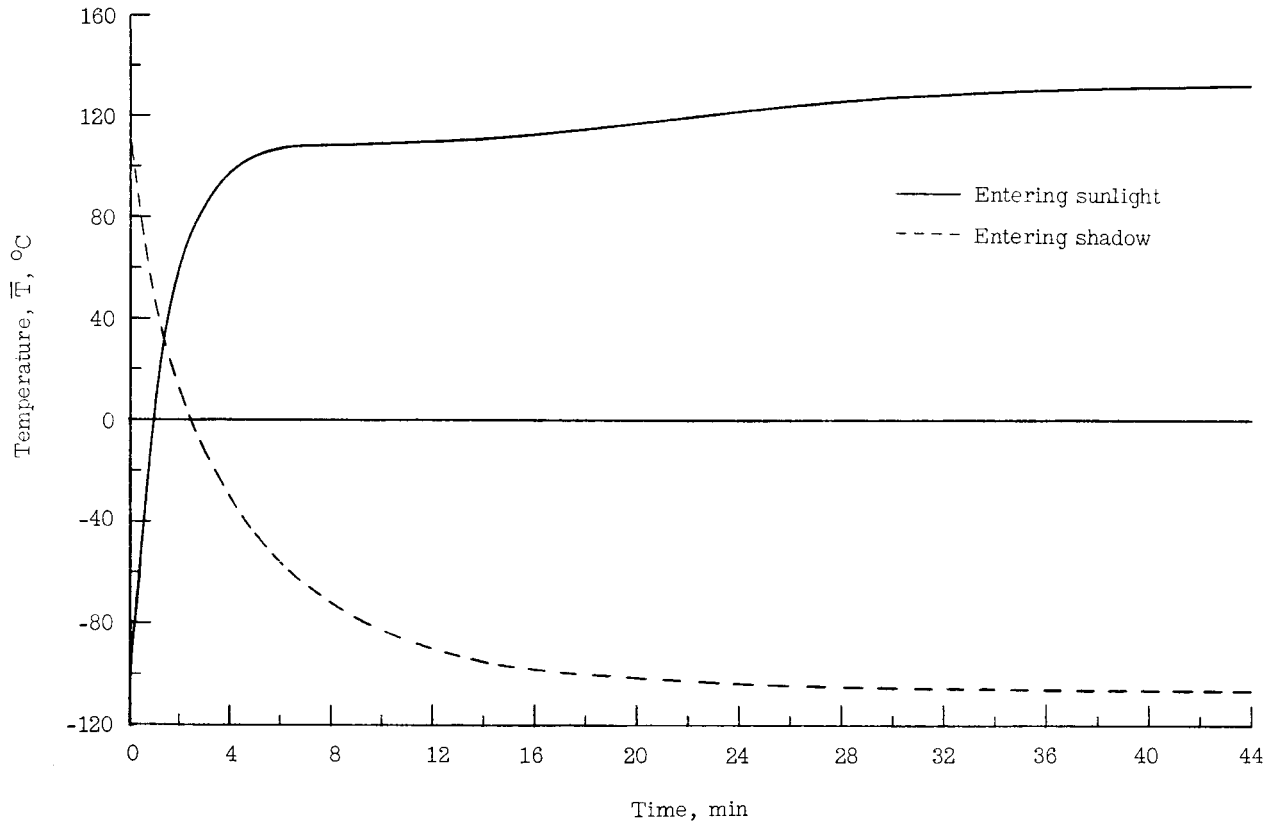

Figure 11.- Predicted thermal response of Echo I as it enters and leaves the earth's shadow.

this curve was taken as the equilibrium or minimum temperature that could be attained in the shadow, the reason being to show the maximum time required for the satellite to reach thermal equilibrium after entering the sunlight. The curve shows a very rapid increase in temperature, that is, from -107° C to 102° C in approximately 6 minutes.

In a circular orbit at an altitude of 1668 kilometers, the satellite travels at a rate of approximately 15° in 5 minutes. It is seen (fig. 9) that the reflected earth radiation does not begin to change the satellite temperature until an angular distance β of about 30° from the shadow has been reached. Therefore, it can be concluded that the satellite has reached thermal equilibrium with its environment after leaving the earth's shadow before the reflected earth radiation becomes appreciable. Because of this rapid thermal response of the satellite, it has been assumed that once the satellite has reached 108° C after leaving the earth's shadow, it remains in thermal equilibrium with its sunlight environment. Hence, temperature increases in figure 11, shown subsequent to 5 minutes after leaving the shadow, are due to increased thermal energy input from the earth-reflected component as the satellite moves toward the sun while in an orbit where δ is 90°.

In calculating these thermal-response characteristics of Echo I, the thermal mass of the inflation powders was not included. The predicted thermal response curves may be considered a bit severe for the initial life of the satellite, but they become more representative of the actual conditions toward the end of the test period when most of the powder has leaked out.

The temperature variations of the satellite have thus far been calculated for sunlight portions of its orbit (fig. 9) as well as for transitions in and out of the shadow (fig. 11). Temperature predictions will next be made for complete orbits. The particular orbits for which these calculations are made can be described by use of the circular orbit geometry seen in figure 5. Calculations were made for arbitrarily selected values of δ of 90°, 60°, 40°, and $\leqq 37.25^{\circ}$ as seen in figure 12. When δ equals 90°, the most severe thermal

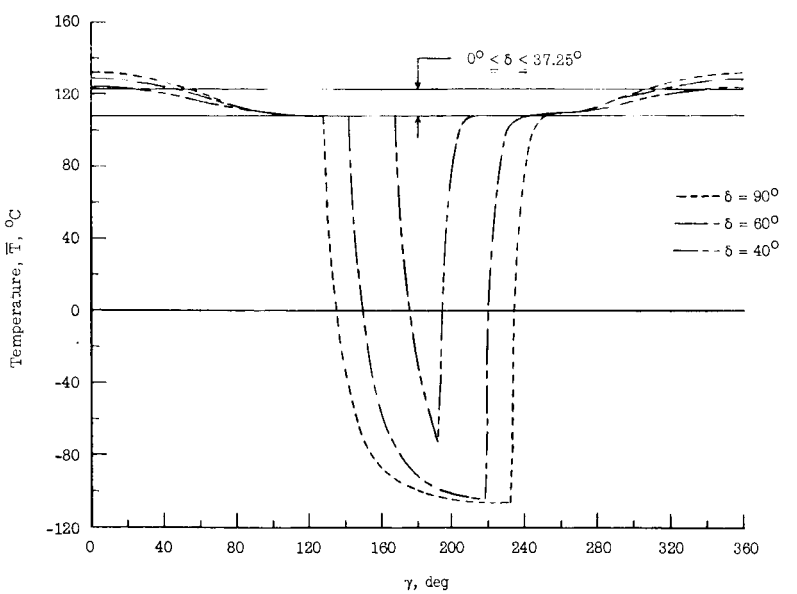

Figure 12.- Predicted variation of Echo I temperature as it traverses orbits where the normal to the orbital plane is inclined at various degrees to the earth-sun line.

excursions will be experienced because the maximum period of time will be spent in the shadow. The satellite will also pass directly between the earth and sun during this orbit and will attain the maximum temperature. The temperature decrease from 132° C to 108° C, seen to occur in the interval $0^\circ \leqq \gamma \leqq 128^\circ$, results from the decrease in earth-reflected radiation. When entering the shadow, the temperature decreases from 108° C to -107° C; whereas when leaving the shadow, the temperature increases rapidly to 108° C with more gradual increase in temperatures above 108° C and reaches 132° C again as it passes between the earth and sun. The variation of temperature around this orbit is from 132° C to -107° C or a change of 239° C. The temperature variations while traversing the orbits of δ equal to 60° and 40° are seen to be over a range of 234° C and 197° C, respectively. For all angles of $\delta \leqq 37.25$ which are continuous sunlight orbits, however, the variation is maintained within the range 108° C to 122° C as indicated by the solid lines in figure 12. As δ decreases from 37.25°, the variations in temperature over a complete orbit will decrease and will become constant at about 110° C when δ is 0°.

These analyses have shown that the satellite will experience very large temperature variations when it passes through even the slightest portion of the earth's shadow as a result of its small thermal mass-to-surface area ratio. Continuous sunlight orbits, on the other hand, can be established with a rather wide degree of flexibility in that the normal to the orbital plane can precess within a solid angle of $2\delta = 76^\circ$ about the earth-sun line for a 1668-kilometer circular orbit, while the satellite will always remain in sunlight and experience average temperature variations in the interval 108° C to 122° C. The hot-spot and coldspot temperatures for these conditions will vary in the interval 124° C to 137° C and 102° C to 117° C, respectively. For these reasons, the Echo I satellite was launched into an orbit such that the satellite would remain in continuous sunlight for the first two weeks; thus the temperature-sensitive pressure-producing subliming compounds would remain effective for the duration of the test period.

Micrometeoroid Impact and Penetration

The Echo I satellite being constructed of such a very thin plastic film is expected to be highly vulnerable to micrometeoroid puncture. All particles with sufficient energy will penetrate through the film and will make small holes through which the inflation gases and vapors can leak out.

Until recently, meteor studies have been limited to photographic and radar echo techniques effective in detecting particles with a mass of about 10^{-4} grams (ref. 4) or greater. With these techniques, the number and velocity can be measured directly while the mass and size can be inferred by some theoretical considerations. In the past few years, rocket and satellite vehicles have afforded the opportunity to perform micrometeoroid impact experiments outside the earth's atmosphere.

The problem as to size and influx of meteoritic particles has been treated in reference 5 with the reservation in mind that the basis for extrapolating the distribution function is not supported by direct evidence. The influx

distribution was determined by beginning with the Millman point (that is, the total number of particles incident on the earth per square meter per second determined by Millman's visual observation) and taking the naked-eye threshold as fifth visual magnitude. The influx of particles is assumed to increase by a factor of $10^{0.4}$ (or 2.512) per magnitude step. The mass distribution was determined by taking the mass of a zero magnitude particle as 25 grams on the basis of the Harvard photographic meteor study (ref. 5) while assuming the mass decreases by a factor of $10^{0.4}$ per magnitude step. This distribution is shown in figure 13 as the theoretical extrapolation.

Direct evidence from micrometeoroid experiments as to the influx of particles with masses of the order of 10^{-9} grams or greater indicates that the influx distribution increases by a slightly higher factor of $10^{0.435}$ (or 2.720) while the mass distribution factor is assumed to remain the same. This new factor is calculated from the experimental extrapolation curve seen in figure 13. It is interesting to note the nearness of this experimentally inferred value of 2.720 to that of the ever-occurring mathematical constant e (that is, e = 2.718).

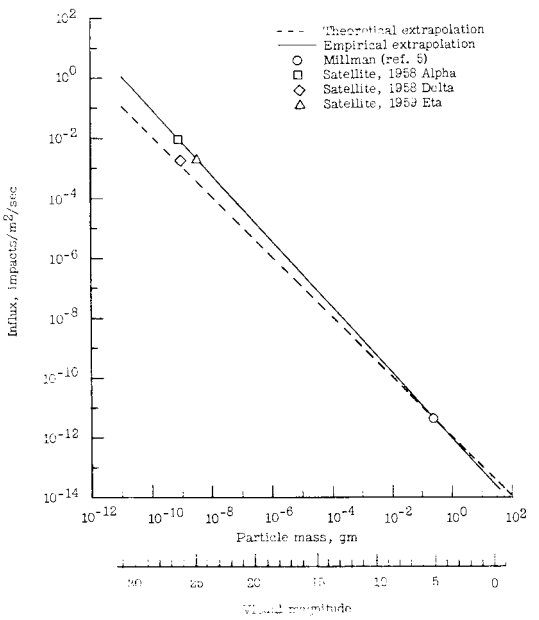

Figure 13.- Comparison of theoretical values with satellite data for micrometeoroid mass and influx distribution.

This curve was constructed by taking the Millman point and the 1959 Eta [Vanguard III] (ref. 6) data points as the most reliable points presently available; the Millman point was chosen because it comes from naked-eye observations and the 1959 Eta point, because it has collected more data from a statistical point of view than any other satellite. Two other experimental points have been plotted in figure 13, 1958 Delta [Sputnik III] (ref. 7) and 1958 Alpha [Explorer I] (ref. 8), the first agreeing somewhat with the theoretical extrapolation and the latter agreeing very well with the Millman - 1959 Eta extrapolation. This agreement further increases the evidence of a higher influx rate than that assumed in the theoretical extrapolation. The satellite data used here were taken from vehicles orbiting at altitudes in the vicinity of the Echo I vehicle. Their apogee-perigee altitudes varied in the interval 300 to 2500 kilometers compared with a circular orbit altitude of about 1668 kilometers for Echo I. This variation is mentioned in light of the possibility that there may be some appreciable variation of influx with altitudes, possibly in orders of magnitude, although there is no evidence to support such a contingency.

An approach to the problem of estimating the rate of hole growth due to micrometeoroids striking the satellite can probably be most easily explained by use of table I (patterned after Whipple's table in ref. 5). The columns have the following meaning:

(1) - Visual magnitude of meteor is shown.

(2) - Mass, grams: The mass is assumed to decrease by a factor of $10^{0.4}$ for each visual magnitude increase step. This relation can be expressed mathematically as

$$m_u = \frac{25}{10^{0.4u}} \tag{22}$$

for each visual magnitude in question.

(3) - Radius, centimeters: The radius of a particle of given mass is calculated by assuming a spherical shape and constant density. The density is assumed to be 2.06 gm/cm^3. This density was calculated from a number of considerations. The recovered meteorites that have been analyzed show a composition of iron and stone. It has been reported (ref. 9) that there are from 4 to 9 times as many stones as irons. If an average composition of 6.5 stones to 1 iron is assumed, an average density of 4.07 gm/cm^3 is calculated. It is reported (ref. 5) that evidence is extremely strong, although not conclusive, that the density of ordinary meteoroids is 0.05 gm/cm^3. If these values are assumed as upper and lower density extremes, the average approximation is taken as 2.06 gm/cm^3. Therefore, the radius of a particle of any visual magnitude can be expressed as

$$R_u = \left(\frac{2.8987}{10^{0.4u}}\right)^{1/3} \tag{23}$$

(4) - Particle cross-sectional area, square centimeters: This number is the cross-sectional area of each particle size calculated from the radii given in column (3) and is seen to be

$$A_u = \left(\frac{16.1284}{10^{0.4u}}\right)^{2/3} \tag{24}$$

(5) - Influx of micrometeoroids on the earth's surface per square meter per second: This number includes all particles of mass equal to or greater than that appearing in the line in question. For any visual magnitude, this number can be expressed as

$$I_u = 3.0480 \times 10^{-14} \times 10^{0.43457u} \tag{25}$$

This number is derived from Millman's observation of 2×10^8 naked-eye meteors striking the earth per day where the threshold of the human eye is taken to be fifth visual magnitude.

(6) - Influx of micrometeoroids on Echo I per second: This number includes all particles of mass equal to or greater than that appearing in the line in question. The number is determined by multiplying one-half the surface area by equation (25). The factor 1/2 is a correction factor necessary to account for the shielding of the satellite by the earth and is valid at altitudes up to about 10^4 kilometers. (See ref. 5.) This number can be expressed as

$$I_u = 4.446 \times 10^{-11} \times 10^{0.4346u} \tag{26}$$

(7) - Influx of micrometeoroids on Echo I for any visual magnitude per second: This number includes all particles within one visual magnitude interval centered around the mass of the particle in the line in question. For example, the line of visual magnitude 10, column (5), gives a number of 6.757×10^{-10} which is a cumulated number of particles and indicates all those with masses of 2.5×10^{-3} grams or greater. The average number of particles of average mass 2.5×10^{-3} grams is determined by assuming one-half the particles between visual magnitude 9 and 10 as well as one-half the particles between visual magnitude 10 and 11 to have this mass. This number can be expressed as

$$I_u = 4.446 \times 10^{-11}\left[\frac{10^{0.4346(u+1)} - 10^{0.4346(u-1)}}{2}\right] \tag{27}$$

(8) - Rate of hole growth in Echo I, square centimeters per second: This number is the rate at which penetration by micrometeoroids with masses of those in the line in question produces holes in the satellite wall through which it passes. The number is calculated by multiplying the cross-sectional area taken from the line in question in column (4) by the average number of particles with the same size taken from column (7).

The total rate of hole growth in the satellite is found by adding the contribution of each size particle with energies sufficient to penetrate through the satellite skin in the visual magnitude interval 0 to 31. Zero will be taken as the upper limit because the probability of a larger particle striking the satellite is negligible, and 31 as the lower limit because the solar radiation pressure will not permit those with smaller energies to exist in the vicinity of the earth. (See ref. 5.) The depth of penetration can be calculated by use of the equation (from ref. 5)

$$d = \left(\frac{9}{\pi\rho'\zeta}\right)^{1/3}\left(E_k\right)^{1/3} \tag{28}$$

where the kinetic energy E_k of the particles is based on a velocity of 15 kilometers/sec for those in the visual magnitude interval 20 to 31. If the density of the film ρ' is taken as 1.38 gm/cm^3 and the heat to vaporization ζ as 4.98×10^9 ergs/gm, equation (28) gives a penetration depth of 1.68×10^{-3} centimeters for particles of visual magnitude 31. This result means that all particles are capable of penetrating the 1.27×10^{-3}-centimeter-thick poly[ethylene terephthalate] film. No micrometeoroid buffer action by the 2,200 angstroms of vapor-deposited aluminum is assumed. By adding the rate of hole area contributions for each visual magnitude in column (8), for lines 0 to 31, it is found that holes will be made in the satellite at the rate of 1.63×10^{-4} square centimeters per second. The penetration depth, given by equation (7), is based on a hole shaped in the form of a right circular cone with total apex angle of 60°. If this shape is assumed to be a fairly accurate approximation of the hole shape actually produced, then it is easily seen that the particles with energies barely sufficient to penetrate but not pass through will not result in holes as large as their cross-sectional area. On the other hand, speculations have been made in this field that indicate a hole larger than the particle cross-sectional area will be produced by particles with sufficient energy to pass through the satellite wall and, in addition, that some of the more energetic ones may pass through the wall twice. These questions and others have led to studies of high-velocity-particle impact phenomena. Thus far, micrometeoroid velocities have not been obtained in laboratories. In view of the questions presently unanswered, an arbitrary correction factor of 2 is assigned to the calculated hole-growth rate; this factor gives 3.25×10^{-4} square centimeters per second which hereafter is taken as the hole-growth rate due to micrometeoroid bombardment in the Echo I satellite.

Deforming Loads

While experimentally evaluating the Echo I satellite as a passive radio relay station, it is necessary that its shape be well defined. The isotropic characteristic of the sphere eliminates any requirement for axial orientation. After the satellite is erected to its spherical configuration, there are four known sources capable of producing deforming loads of sufficient magnitude to warrant consideration: (1) The atmospheric molecules will develop a static pressure as well as a dynamic pressure, (2) impinging micrometeoroids will produce a pressure, (3) the sun will develop a solar radiation pressure, and (4) the memory that the satellite retains of its folded condition can cause preferential deformation of the surface along fold lines.

Static atmospheric pressure.- The static pressure of the atmosphere up to an altitude of 700 kilometers is taken from reference 10. An extrapolation has been made in the interval 700 to 2000 kilometers. The results can be seen in figure 14.

Dynamic atmospheric pressure.- The dynamic pressure under consideration is that pressure developed at the stagnation point. It is assumed that the mechanical interaction between the atmospheric molecules and the satellite is purely elastic. This assumption simplifies the analysis and results in a conservative estimate in light of the objective, which is to show eventually that

the inflation and pressure sustenance system will be expected to keep the satellite in a spherical shape for the 1- to 2-week test period. Free molecular flow will exist at the altitudes of interest where the mean free path is of the order of hundreds of kilometers. Under these conditions the number of molecules striking the satellite per unit surface area at the stagnation point will be

$$nv_B t \tag{29}$$

The momentum transfer of each of these molecules will be $2mv_B$, if the satellite velocity is assumed to be much greater than the thermal velocity of the molecules. The time rate of change of the momentum will be

$$\frac{(nv_B t)(2mv_B)}{t} \tag{30}$$

This relation is recognized as the impulsive force from which the pressure or force per unit area can be written as

$$p = 2\rho v_B^2 \tag{31}$$

where ρ is the atmospheric density. The satellite velocity for a circular orbit is

$$v_B = \sqrt{\frac{g_o R_E^2}{R_E + h}} \tag{32}$$

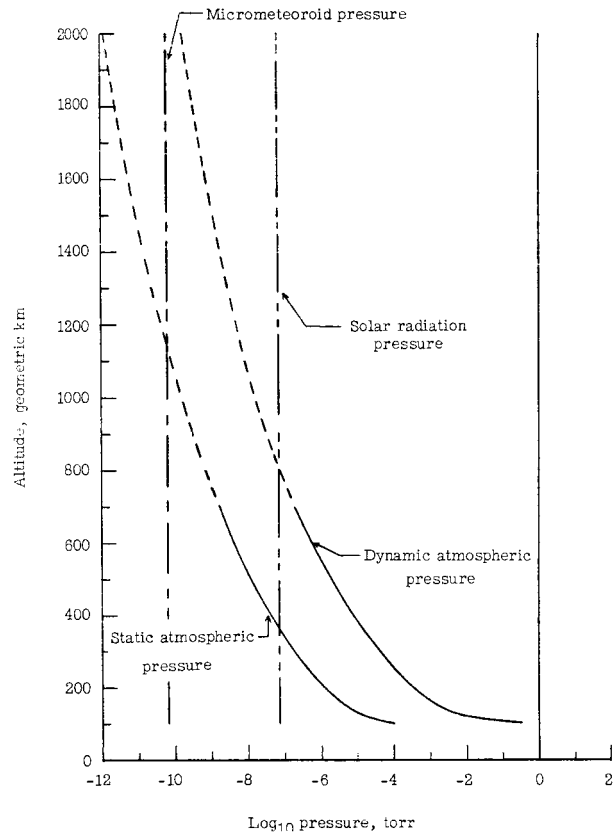

Figure 14.- Comparison of four sources of external pressure above 100 kilometers altitude.

The densities up to an altitude of 700 kilometers were taken from reference 4 and extrapolated from 700 to 2000 kilometers. By substituting these densities and the velocities from equation (32) into equation (31), the dynamic pressure was calculated and can be seen in figure 14. It will be noticed from this figure that the static pressure is about one-hundredth that of the dynamic pressure above 600 kilometers. In a 1668-kilometer circular orbit, the dynamic pressure at the stagnation point is found to be 5.624×10^{-10} torr.

Micrometeoroid pressure.- The pressure resulting from the impingement of micrometeoroids on the surface of a satellite can be estimated on the basis of the number and size distribution of cosmic dust particles believed to exist in the earth's vicinity of space. It will be assumed that the impacting micrometeoroids are distributed uniformly over a plane surface normal to the direction of motion, have a uniform spatial distribution, and that the particles are stopped completely by the surface. The satellite velocity is neglected in

computing the momentum change of the particles since it is only about one-third the micrometeoroid velocities of 15 to 28 kilometers per second given in reference 5. Based on these assumptions, the pressure resulting from this source can be computed from the time rate of change of the particles' momentum per unit of surface area which is

$$p = \sum_{u=0}^{u=31} n_u m_u v_u \tag{33}$$

The magnitude of n_u can be determined by dividing column (7) in table I by half the Echo I surface area, m_u can be taken directly from column (2) in table I, and v_u is obtained from reference 5. The pressure computed from equation (33) is 6.48×10^{-11} torr which is considered a maximum value applicable to Echo I from this source because the particles all have sufficient energy to pass through the thin film used for fabrication; hence all their momentum will not be given up at the surface. This pressure is seen (fig. 14) to be independent of altitude and about one order of magnitude less than the dynamic atmospheric pressure at Echo I altitude.

Solar radiation pressure.- The solar radiation pressure is proportional to the normally incident energy flux C_S taken as 1.395×10^6 ergs/cm^2-sec at 1 astronomical unit from the sun. An equation for expressing the pressure produced by this radiation is given in reference 11 as

$$p_n = \frac{2C_S}{c} \tag{34}$$

In the derivation of this equation, it was assumed that the solar energy was incident normal to the surface of a perfectly specular reflecting mirror. The surface of the satellite approaches these conditions. There will always be a point on the surface where the radiation is at normal incidence due to the satellite's spherical symmetry, and although the vapor-deposited aluminum surface absorbs about 10 percent of the incident solar radiation, the pressure predicted by equation (27) can be considered as an upper limit as a result of this source. From equation (34) it is found that the solar radiation pressure is 6.91×10^{-8} torr or 123 times as great as the dynamic atmospheric pressure at an altitude of 1668 kilometers. This pressure is plotted as a constant in figure 14 for futher comparison of the deforming pressures present in the environment of space. It is interesting to note that the solar radiation pressure is greater than the dynamic atmospheric pressure above about 800 kilometers and greater than the static atmospheric pressure above about 360 kilometers.

Memory of folds.- As the satellite is compactly folded and packaged into its 67.31-centimeter container, folding angles of 180° are made. The folds are all subjected to a 1-atmosphere loading during the packaging process by placing the folded balloon inside a plastic bag and evacuating the bag so that the external atmospheric pressure will compress it to a minimum size. This process yields the plastic film along the fold lines so that when the load is removed it is left permanently set. When the satellite is inflated, it will retain a memory of these folds unless the material is again yielded after the satellite

becomes spherical. It would require about 58.96 kilograms of benzoic acid to produce an internal pressure large enough to stress the film skin to its 8.96×10^8 dyne/cm^2 (ref. 12) yield point. Since this weight far exceeds the payload weight limitations, the alternate solution of maintaining a positive internal pressure was employed.

The critical buckling pressure of a smooth thin-wall sphere can be determined theoretically from the equation

$$p_{cr} = \frac{2Et'^2}{R^2\sqrt{3\left(1 - \nu^2\right)}} \tag{35}$$

taken from reference 13. If it is assumed that Echo I is such a smooth sphere, this pressure is found to be 2.28×10^{-5} torr, where the modulus of elasticity of the film was taken as 3.80×10^{10} dynes/cm^2 (ref. 12) and Poisson's ratio was assumed to be zero.

From this analysis of deforming loads, it can be seen that the critical buckling pressure of the Echo I satellite based on equation (35) is much greater than the deforming pressures present in the environment of space. However, the memory effect of this satellite makes it imperative that a small skin stress be maintained to prevent the surface from collapsing. If it were possible to remove the memory, the satellite would not require a sustained pressure to maintain sphericity nor would it be expected to buckle (on the basis of eq. (35)) until it had come down to an altitude of about 250 kilometers.

INFLATION MEDIUM

Considerations

In the design of an inflation system for large, inflatable satellites, the prime considerations are that it be simple, lightweight, and reliable. The inflation system must be initiated after the satellite has been transported through the dense atmosphere of the earth inside a closed container and released in orbit into the vacuum of space. Past conventional methods of inflation have utilized compressed gas where the bottles and ejection system consume most of the inflation-system weight; the bottles, however, are susceptible to leakage and are difficult to store. A system based on the sublimation principle is investigated herein and is predicted to be quite satisfactory. In this application no bottles are used and the inflation compound is distributed inside the sphere in a loose powder form in such a manner that it lends itself very well to folding and packaging techniques.

Careful consideration must be given to the amount of residual air that can be tolerated inside the packaging container yet outside the balloon, as well as the amount of air left inside the balloon. If the container were closed with 1 atmosphere absolute pressure inside, the balloon would virtually explode when released in the vacuum of space. Appreciable moisture or other volatile condensables inside the balloon would also result in rather explosive inflation. To prevent either of these occurrences, the container for the Echo I satellite

was designed to maintain a vacuum. It was determined experimentally that a pressure of 1 to 3 torr could be tolerated inside the container without resulting in too rapid inflation as well as being low enough for the moisture content to evaporate and be pumped away during the evacuation process of the canister. This pressure is sufficiently high to prevent the low vapor pressure inflation compounds from subliming out of the folded balloon through the small holes placed in it to allow the water vapor and residual air to be pumped away during the evacuation. There were 244 holes, hereafter referred to as air orifices, placed in the sphere, 1.59 millimeters diameter, and located along the outside of each fold to allow air flow with a minimum amount of restrictions during the evacuation. These holes had a total area of 4.84 square centimeters.

When it is necessary, as in the case for Echo I, to maintain a pressure inside the satellite after inflation, the inflation system weight can be utilized more efficiently by using two subliming compounds. One of the compounds was used for generating a sufficiently high vapor pressure to break the unfolding loads and erect the balloon to its full size, and a second compound with a lower vapor pressure, under the same temperature conditions, to maintain inflation for the desired period of time. The lower vapor pressure compound will not be lost as fast through the air orifice and micrometeoroid holes in the skin as the more volatile, initial inflation compound; thus, less weight is required.

The vapor pressure of a subliming compound in solid-vapor equilibrium varies according to the integrated Clausius-Clapeyron equation which is

$$p = c'\exp\left(-\frac{\lambda}{R_g T}\right) \tag{36}$$

It will be noted from this relation that the equilibrium vapor pressure of the compound increases exponentially as its temperature increases linearly, the assumption being made, of course, that the latent heat of sublimation remains constant over the range of interest. This condition suggests that a subliming compound can be chosen with a low equilibrium vapor pressure at room temperature (20° C) which will have a much higher equilibrium vapor pressure when the satellite is deployed in space and is subsequently heated from the direct solar, earth-reflected solar, and direct earth radiant heat input. As the temperature of the subliming powder inside the satellite rises, its vapor pressure will rise to such a point that the satellite begins to unfold. To compensate for volumetric expansion during inflation, the subliming powder will act as a gas generator to maintain vapor pressure equilibrium.

The rate of inflation from the time the satellite is released in the vacuum of space until it reaches full size will depend primarily upon the residual air left inside the satellite, the sublimation rate of the powder, and the mechanical forces required to unfold and erect the sphere. The rate of inflation resulting from the subliming of the powders is dependent on both the geometric cross section and the effective solar absorptivity of the satellite which are interdependent and do not lend themselves to any known degree of reliable prediction. The time that it takes for inflation, however, can be determined with a fair degree of accuracy by experimental methods.

Radar signals returned from the inflating sphere will display a high degree of scintillation while inflation is occurring. Once the inflation motion ceases, the radar return should exhibit no scintillation after it has been corrected for any periodic low-frequency satellite spin scintillation. These data will give a fair approximation as to the degree of inflation by estimating the geometric cross section from the radar cross section. The accuracy of this method increases with degree of inflation and should be excellent at 100-percent inflation.

Even though the transient inflation is governed by a number of interdependent parameters that do not lend themselves to current theoretical analysis, the fully inflated state can be investigated by a rather straightforward method. The internal pressure required for a thin-wall spherical satellite is determined from the desired stress level in the skin and can be calculated from

$$p_i = \frac{4t'S}{D} + p_o \tag{37}$$

If the internal pressure required and the temperature environment in which the subliming compound must function are known, a compound can be selected that best satisfies these conditions.

There are perhaps four potential sources of pressure generation that are, to a large extent, inherently associated with an inflatable structure of this nature that should be considered. These sources are (1) the expanded atmospheric gases left inside the sphere during packaging, (2) desorbed gases from the fabrication material, (3) thermal radiation within the sphere, and (4) the vapor pressure of the fabrication material.

The expansion of the free atmospheric gas can be computed from the volumetric expansion during inflation by assuming an isothermal transition to give maximum residual pressure. The volume inside the Echo I sphere increases by a factor no less than 1.3×10^5 with a resulting pressure no greater than 2.31×10^{-5} torr based on an initial pressure of 3.0 torr.

Atmospheric gases and vapor (adsorbates) attached to the inside surface of the packaged sphere may be partially or completely desorbed when the satellite is released in space, inflated, and heated. Adsorbates are usually assumed to be attached to the surface of solids by nonspecific forces of attraction between gas and solid such as Van der Walls forces that give rise to physical adsorption and by chemical bonds formed between the gas and solid generally referred to as chemisorption. As a general rule when the adsorbates are below their critical temperature, multilayer adsorption takes place through both physical and chemical bonding whereas at higher temperatures chemisorption only occurs and is usually limited to monolayer thickness. (See ref. 14, ch. IX.) Since water vapor is the only adsorbate present in the atmosphere during satellite preparation that has a critical temperature greater than normal room temperature (that is, 20° C), it will be most susceptible to the more consequential multilayer adsorption. It has been further observed through the study of the isothermal adsorption characteristics of adsorbates that, generally, monomolecular, adsorption prevails at pressures of 0.1 or less than that of saturation, whereas multilayer adsorption prevails at higher pressures and increases with increasing

pressure until saturation is reached. (See ref. 14, p. 519.) For lack of a more quantitative approach to predicting the adsorption and absorbate characteristics of the solids and adsorbates in question, a prediction is made on the qualitative analysis presented.

The partial pressure of water vapor inside the Echo I canister must be less than the 1 torr to 3 torr absolute pressure permitted which is approximately 0.1 of the 17.5-torr saturation pressure; this requirement places it in the monomolecular adsorption region. The pressure increase resulting from desorption of these adsorbates can be expressed as

$$p = \frac{Nk'T}{V_B} \tag{38}$$

where N is the total number of molecules desorbed. If the monomolecular covering power of water vapor is taken as $5.27 \times 10^{14} \frac{\text{molecules}}{\text{cm}^2 - \text{monolayer}}$ (ref. 15, p. 36), equation (38) can be rewritten as

$$p = \frac{162.796j}{D_B} \qquad (j \geqq 1) \tag{39}$$

per monolayer of desorbed water where j is the ratio of microscopic surface area to apparent surface area. Since the plastic film is a continuous sheet essentially free of pinholes (ref. 12, p. 2,293) j will be taken as 1.0 and the pressure inside the Echo I sphere produced by a monolayer of desorbed water vapor will be 4.0×10^{-5} torr.

The pressure produced inside a thin-wall spherical shell as a result of the inherent emission, absorption, and reflection of thermal energy from its surface can be calculated by use of equation (34). For the purpose of simplifying the computation, the spherical shell is assumed to be at thermal equilibrium with its environment with an isothermal temperature prevailing over the entire surface. Radiation interaction inside the sphere can be assumed to be radially symmetric over the entire surface and producing a uniform pressure outward, and the radiation emitted from the outside is assumed to be radially symmetric over the surface and producing an inward pressure acting against the pressure produced within. The pressure produced on the inner surface can be expressed as

$$p_i = \frac{2\epsilon_i \sigma T^4}{c} \tag{40}$$

where the factor of 2 accounts for the fact that thermal energy is absorbed at the same rate that it is emitted at equilibrium. The uniform and symmetric pressure produced on the outside surface is

$$p_o = \frac{\epsilon_o \sigma T^4}{c} \tag{41}$$

The net uniform thermal radiation pressure produced will then be

$$p_T = \frac{\left(2\epsilon_i - \epsilon_o\right)\sigma T^4}{c} \tag{42}$$

There are also thermal radiation pressures from other sources produced on the outside surface of the sphere; however, they are asymmetrical and were considered in an earlier section with other deforming loads. The differential thermal radiation pressure produced inside Echo I where ϵ_i is 0.45 and ϵ_o equals 0.03 is computed from equation (42) to be 2.21×10^{-8} torr.

A search of the literature revealed very little information with regard to the absolute vapor pressure of the plastic film used for Echo I. Reference 16 reports that the vapor pressure of the material can be expressed as

$$\log_e p = 14.103 - \frac{6908}{T} \tag{43}$$

where the constants were determined empirically to satisfy the pressure-temperature relations measured over the range 27° C to 177° C. The pressures, however, are reported to have been measured with an ionization-type gage that was calibrated in a nitrogen atmosphere. An interpretation of the pressure derived from equation (43) as vapor pressure, in the usual sense of the term, would be unjustified. This equation gives a pressure of 1×10^{-7} torr at 25° C and 3×10^{-5} torr at 125° C. A second reference (ref. 17) states that theoretical calculations of the vapor pressure of the lowest molecular weight fraction to be found in poly[ethylene terephthalate] plastic film indicate that at a temperature of 125° C, the vapor pressure will be approximately 10^{-40} torr. The plastic film was also subjected to a 5×10^{-7} torr vacuum to determine the weight loss. In general, vacuum exposure of the film at room temperature for periods up to 1,419 hours resulted in less than 0.1-percent loss in weight. Reference 17 indicates that the vapor pressure of this film is much lower than those of reference 16; therefore, volatile products of the film will be neglected as a source for producing pressure of a magnitude of concern inside the Echo I satellite.

Summing the pressures from these four more or less inherent sources gives a total pressure inside the sphere when it is fully distended of only 6.31×10^{-5} torr. This pressure would produce a skin stress in the Echo I sphere of only 5.03×10^4 dynes/cm^2 which is much too small to effect reliable inflation.

Vapor Pressure of Compounds

The vapor-pressure—temperature relations for compounds at low temperatures are difficult to find in the literature; therefore extrapolation is

necessary in most cases. Table II contains the vapor-pressure—temperature relations as well as other useful physical properties for a number of organic compounds. The equation

$$\log_e p = A' - \frac{B'}{T} \tag{44}$$

for which the constants A' and B' have been calculated and listed in the table is a simplified version of a second form of the Clausius-Clapeyron equation (ref. 18)

$$\log_e \frac{p}{p_o} = \frac{\lambda}{R_g}\left(\frac{1}{T_o} - \frac{1}{T}\right) \tag{45}$$

Equation (44) has been plotted in figure 15 for all the subliming compounds listed. It is pointed out that the curves are extrapolated outside the temperature intervals listed in table II; this condition means, of course, that the latent heat of sublimation has been assumed to be constant.

Selecting the Compound

The organic class of compounds has been selected because they generally exhibit vapor-pressure—temperature characteristics in the range of interest. In selecting the compound, a number of considerations must be made: (1) it must satisfy the pressure-temperature requirements, (2) the melting temperature must be higher than any temperature expected while the satellite is packaged inside the container to prevent liquid flow which could unbalance the payload (this consideration is very important when launching with a spin-stabilized vehicle), (3) the lowest molecular weight possible should be selected to minimize weight requirements, (4) it must be nontoxic for safety of handling, (5) it must be noncaustic, and (6) it must be available in large quantities.

From these considerations, benzoic acid and anthraquinone were selected as two inflation compounds for the Echo I satellite: the benzoic acid to serve as the initial inflation compound and the anthraquinone to serve as the pressure-sustaining compound for the 1- and 2-week test period. In discussing the pressures that will be developed and the quantity of each of these powders required, the temperature of the satellite will be taken as 102° C which is the minimum coldspot temperature previously determined (fig. 9) for a continuous sunlight orbit. From calculations previously made, it can be seen that for continuous positive internal pressure to be maintained, the satellite must remain in a continuous sunlight orbit during the test period because of the rapid thermal response of the satellite and subsequent decrease if the compound's vapor pressure of the earth's shadow should be entered.

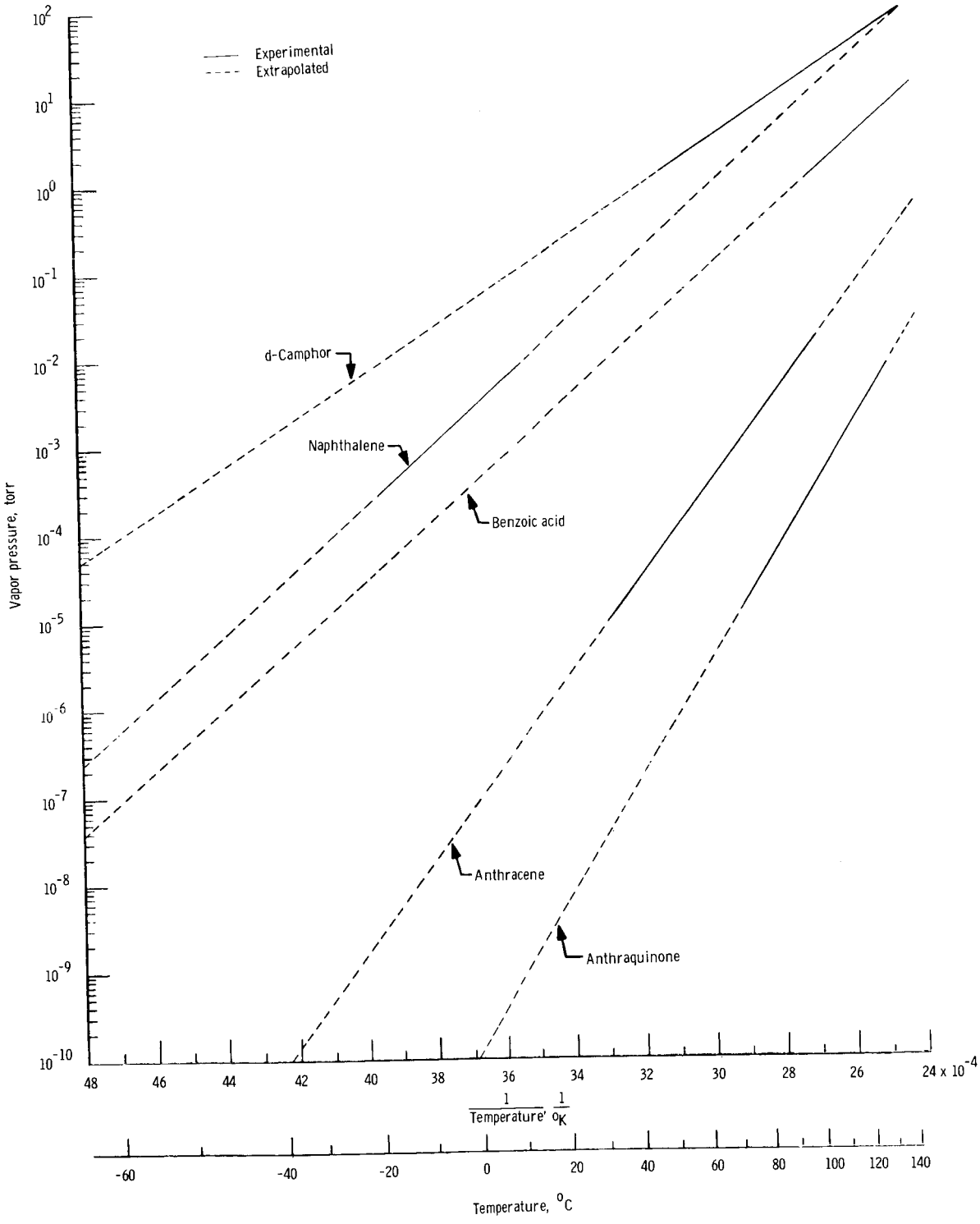

Figure 15.- Vapor pressure characteristics of some organic compounds.

Quantity of Compound

The maximum quantity of initial inflation compound that can be tolerated inside the satellite is limited by the maximum permissible skin stress when the satellite is full size. For instance, if the benzoic acid used in Echo I were permitted to reach pressure equilibrium between the solid-vapor phase at 102° C, a pressure of about 2 torr, derived from equation (44), would be attained. This pressure would develop a skin stress of 1.59×10^9 dynes/cm^2 in a fully inflated Echo I. A rupture in the satellite would occur under these conditions since the tensile strength of the skin material of approximately 1.03×10^9 dynes/cm^2 would be far exceeded. Figure 16 contains pressure-temperature relations for various quantities of benzoic acid over a wide range

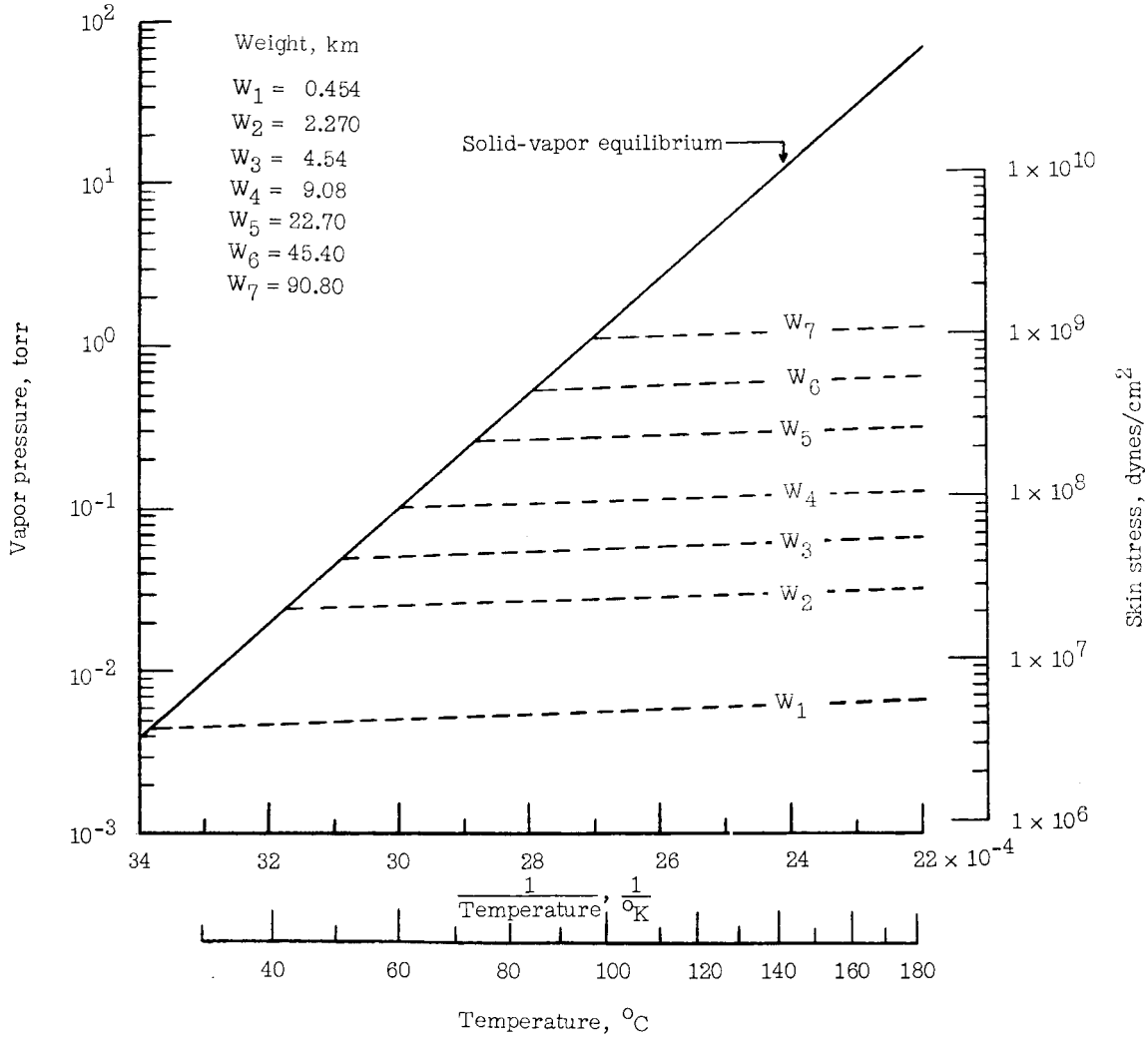

Figure 16.- Temperature-dependent pressure and skin stress that would result in Echo I satellite by use of various quantities of benzoic acid.

of temperatures. The solid-vapor equilibrium curve is determined from the relation

$$\log_e p = 29.59 - \frac{8223}{T} \tag{46}$$

by assuming an unlimited supply of the solid. The curves labeled $W_1, W_2, \ldots$, etc., are determined from the ideal gas law

$$p = \frac{WR_gT}{MV} \tag{47}$$

which will prevail when all the solid has changed to the vapor phase. For example, it is seen that by using 2.27 kilograms of benzoic acid, the pressure would rise rapidly along the solid-vapor equilibrium curve until the point of intersection with W_2 is reached, from which point further increase in temperature would result in only slight pressure increases along W_2. On the other hand, if 45.40 kilograms were used, the pressure would increase to a much higher value before it leveled off along W_6. The corresponding skin stress determined from equation (37) is shown along the right-hand side of the figure.

Controlling the quantity of inflation compound is an excellent means of controlling the maximum skin stress in the satellite without having to be concerned with controlling the equilibrium temperature so that it does not go higher than that actually required. It was determined experimentally that a somewhat arbitrarily selected skin stress of about 3.5×10^7 dynes/cm^2 in the Echo I satellite would result in a very taut mirror-surfaced sphere. It is seen (fig. 16) that 4.54 kilograms of benzoic acid would satisfy this requirement and would produce about 4.77×10^7 dynes/cm^2 skin stress while operating at the previously determined temperature of 102° C.

Since 4.54 kilograms of benzoic acid is required for the initial inflation compound, 9.08 kilograms of the allocated inflation system weight is left for the anthraquinone, the pressure-sustaining compound.

Pressure Time History

The pressure time history of the satellite is predicted for a continuous sunlight orbit where the coldspot equilibrium temperature is taken as 102° C. The loss of inflation vapors from the satellite is assumed to be entirely through air orifice holes totaling 4.84 square centimeters and holes produced by micrometeoroids at the rate of 3.25×10^{-4} square centimeters per second. Loss of vapors through permeation of the satellite wall has been considered. However, based on the small diffusion rate of helium gas through the material reported in reference 19, this mode of vapor escape will be assumed to be negligible compared with the others. Reference 19 reports a permeability

constant of the film to helium gas at standard conditions of temperature and pressure of 0.032×10^{-10} cm^3-cm/(sec-cm^2-torr) at 0° C, which was found to increase exponentially with increasing temperature as expected. The diffusion rate of helium through the Echo I sphere would be 1.32×10^{-3} milligrams per second at 0° C based on a differential pressure of 0.10 torr and a film thickness of 1.27×10^{-3} centimeters. A permeation rate of about 4×10^{-2} milligrams per second at 100° C can be predicted for helium based on an extrapolation of the reported data. By assuming the same permeability constant for benzoic acid, a permeation rate at 100° C of 1.2 milligrams per second would be expected as a result of the larger molecular weight. The permeation rate of helium through a seal of the same type used to connect the Echo I gores was reported in reference 19 to be less than that through the basic material. The thin film of aluminum deposited on the outside surface of the Echo I fabrication material would tend to reduce this rate of permeation even further.

Comparison of the initial partial pressure of benzoic acid (fig. 16) at the satellite equilibrium temperature and the vapor pressure of anthraquinone (fig. 15) at the same temperature indicates that the anthraquinone produces a partial pressure only 1/65 as great as benzoic acid and can be considered to be negligible as far as the initial maximum internal pressure is concerned. However, as the more volatile benzoic acid leaks out of the satellite through the air orifice and micrometeoroid holes, its partial pressure will decrease rather rapidly and soon reach the same order of magnitude as that of the anthraquinone pressure-sustaining compound. The anthraquinone will maintain a constant partial pressure of 1×10^{-3} torr by subliming at the same rate that its vaporized molecules flow out of the satellite until all the solid is gone. At this time, its partial pressure will decrease rapidly.

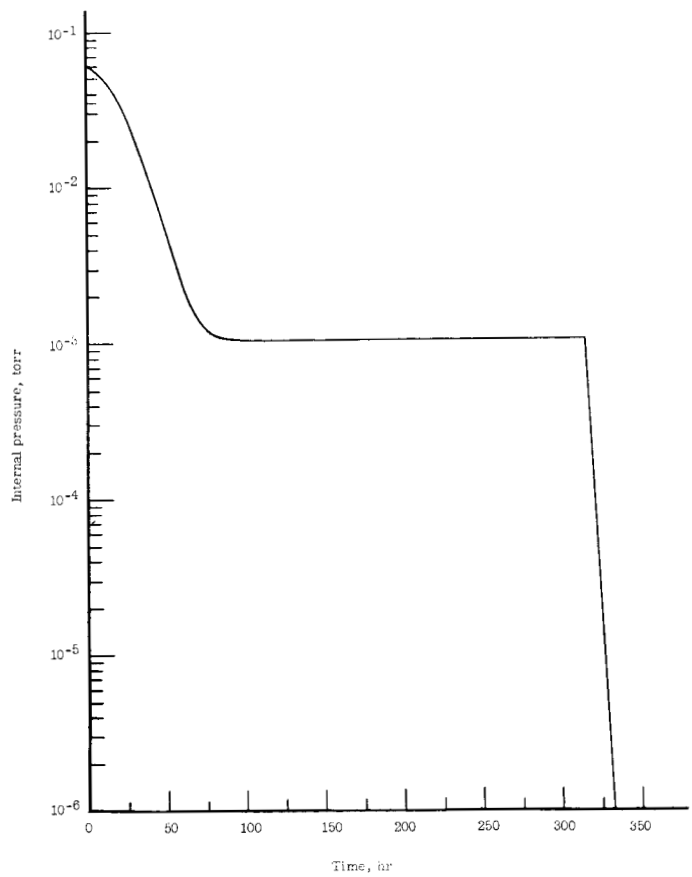

Figure 17.- Predicted internal pressure history inside Echo I satellite from use of 4.54 kilograms of benzoic acid and 9.08 kilograms of anthraquinone.

An equation for expressing the pressure time history inside a vessel (maintained at constant volume and constant temperature) occurring as a result of free-molecular-flow leakage is derived in appendix B as

$$p = \frac{p_o}{\exp\left[C'\left(ft + \frac{1}{2}gt^2\right)\right]} \qquad (48)$$

This equation describes the partial pressure of a sublimed vapor only if the compound under consideration is all in the vapor state and therefore the molecular flow out is not replenished by further sublimation. The benzoic acid will satisfy this condition at the time of full inflation. By summing the resultant pressure of equation (48) for benzoic acid and the constant pressure of 1.0×10^{-3} torr for anthraquinone, the total internal pressure is determined and appears in figure 17. It is seen from this curve that the pressure decreases from about 6×10^{-2} torr to the 1.0×10^{-3} torr partial pressure of anthraquinone in about 100 hours. After this time, the partial pressure of benzoic acid is negligible compared with that of the anthraquinone. From 100 to 315.6 hours, the anthraquinone maintains a constant pressure because of its gas generation action in order to maintain vapor pressure equilibrium. The pressure decreases sharply at the end of 315.6 hours. This decrease results from the fact that at this time there no longer remains any anthraquinone in the solid state and its resultant pressure will obey equation (48). The pressure decreases much more rapidly at this time than it did for the benzoic acid initially. This condition is explained by the fact that the accumulated micrometeoroid holes are much greater at the end of 315.6 hours than during the time the benzoic acid was escaping.

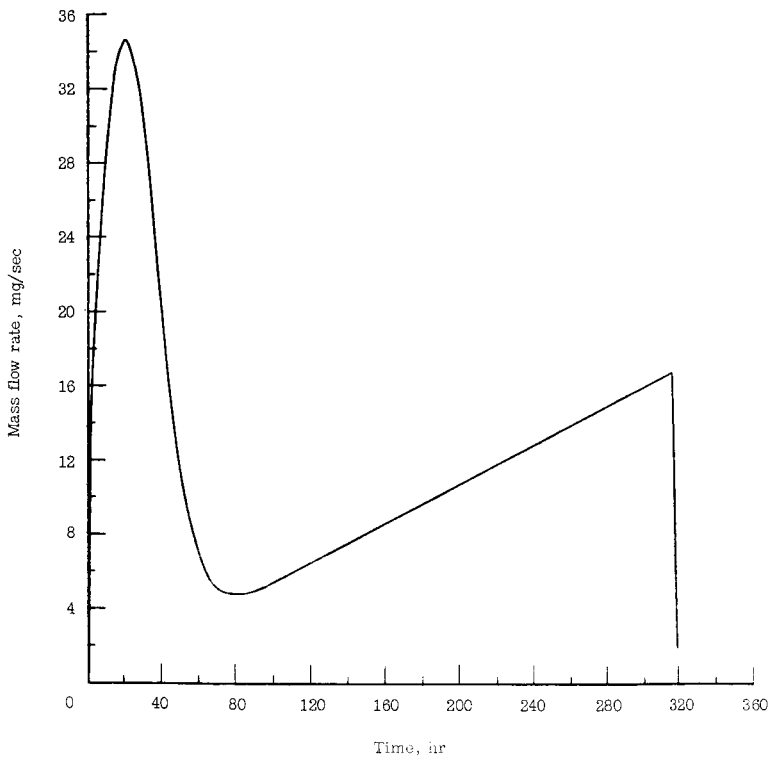

Figure 18.- Predicted mass flow rate of the inflation compounds, benzoic acid, and anthraquinone, from Echo I satellite while in a continuous sunlight orbit.

The period of time that the pressure-sustaining compound will maintain constant pressure is obtained by first determining, by use of equation (47), the quantity of compound that must be in the vapor state for vapor pressure equilibrium to exist. For anthraquinone at 102° C, it is found that 135 grams is required. Next, the time required for all but 135 grams of the compound to flow out is determined (see eq. (B1)) to be 315.6 hours. The general equation for determining this period of time is

$$m - \frac{pVM}{R_gT} = 4.375 \times 10^{-5} p\sqrt{\frac{M}{T}}\left(ft + \frac{1}{2}gt^2\right) \tag{49}$$

(which was obtained by integration of equation (B1)). The first term on the left-hand side of the equation is the quantity of pressure-sustaining compound placed inside the satellite; the second term is the quantity required in the vapor state for equilibrium pressure to exist. The difference between these two terms is the quantity of compound that can flow out before all the solid is gone. For constant pressure, volume, and temperature conditions, which will be the case as long as the satellite does not enter the earth's shadow, equation (49) is recognized as a quadratic which is easily solved to give the period of time that the partial pressure of the pressure-sustaining compound will remain constant.

Mass Flow Rate

In the interest of orbital perturbation and precession calculations for Echo I, the mass flow rate out of the satellite is plotted in figure 18. This curve is determined from (see appendix B),

$$-\frac{dm}{dt} = 4.375 \times 10^{-5} p\sqrt{\frac{M}{T}}(f + gt) \tag{50}$$

The rate at which each of the compounds flows out of the satellite is treated separately because their pressures vary independently. By summing the independent mass flow rates as a function of the compounds' partial pressures, as determined from the pressure time history calculations, the equation for the total mass flow rate up until the time when the solid anthraquinone disappears is

$$-\frac{dm}{dt} = 4.375 \times 10^{-5}\left\{\frac{p_{o,b}\sqrt{\frac{M_b}{T}}}{\exp\left[C'\left(f + \frac{1}{2}gt^2\right)\right]} + 1.33\sqrt{\frac{M_a}{T}}\right\}(f + gt) \tag{51}$$

At the time 315.6 hours (fig. 17) when there is no anthraquinone remaining in the solid state, its mass flow rate will decrease rapidly according to equation (50), where the pressure is decreasing as determined in the pressure time history analysis.

The curve in figure 18 shows a very rapid increase in mass flow rate initially. This increase results from the initial vapor pressure of benzoic acid and the increase in leakage due to micrometeoroid puncture. At about 20 hours, the mass flow rate decreases rapidly since by this time the micrometeoroid holes have accumulated to such size that the rate of partial pressure decrease has become the controlling mass flow rate parameter rather than the micrometeoroid hole growth rate. Between 70 and 90 hours, there is a second sudden

change in the slope of the curve. During this time the supply of benzoic acid is depleting, and the anthraquinone is the predominant vapor flowing out of the satellite. Since its vapor pressure remains constant from the time $t = 0$ to $t = 315.6$ hours, its rate of flow is governed entirely by the rate of micrometeoroid hole growth and will show a linear increase as seen from the curve. At the end of 315.6 hours, the rate of flow decreases very rapidly since the supply of solid anthraquinone that has been generating vapor at the same rate as that lost through leakage is now also depleted. Therefore, constant pressure can no longer be maintained.

Throughout the pressure time history and mass flow rate analysis, the external pressure has been assumed to be negligible. This assumption is valid throughout the investigation since the internal pressures have not been of interest below about 10^{-6} torr, which is 2 orders of magnitude higher than the external pressures. (See fig. 14.)

ORBITAL RESULTS AND DISCUSSION

The Echo I satellite was launched from the Atlantic Missile Range aboard a three-stage Thor-Delta vehicle at 09:39:42 Greenwich mean time (G.m.t.) on August 12, 1960. It was injected into a nearly circular orbit with an inclination of 47.24°. The apogee and perigee of the orbit were at 1688 and 1522 kilometers, respectively, and were very near the 1668-kilometer circular orbit attempted. The satellite successfully inflated within about 10 seconds after it was released from its container and remained in continuous sunlight for 12 days. The satellite entered the shadow for the first time at 09:23:42 G.m.t. on August 24, 1960.

Experimental evidence from the radio-scattering characteristics of the satellite (ref. 20) indicates that its sphericity began to degrade from 6 to 12 days after launch. Six days were indicated by data taken over large bistatic scattering angles between stations on the west and east coasts of the United States and 12 days indicated by data taken over much smaller bistatic scattering angles (the bistatic scattering angle is the included angle between transmitter, satellite, and receiver). The 12 days agree favorably with the 13 days predicted for the pressure-sustaining anthraquinone to leak out; however, this time is also the time that the satellite entered the earth's shadow for the first time. Since all the more volatile benzoic acid would have leaked out by this time, the vapor pressure produced by the remaining anthraquinone may not have been sufficient to push the satellite walls back out to full size after it had experienced a period of partial collapse while in the shadow of the earth.

It is reported in reference 20 that the experimental data indicate that "as of March 1, 1961, Echo I was probably an approximately spherical object with a diameter no less than 70 feet (21.355 meters) and with a somewhat wrinkled skin. There may be a few flattened areas, as indicated by rare deep fades in the radar signal, but it is evident that it could still be used for voice communications."

CONCLUDING REMARKS

The investigations made herein have shown that inflation of large, thin-wall spherical satellites is practical and has been successfully employed in the inflation and pressure sustenance of the Echo I satellite.

The inherent thermal characteristics of the satellite were such that the minimum skin temperature would stabilize at about 102° C while in a continuous sunlight orbit. The coldest temperature of about -106° C would be expected during a maximum shadow transition with very rapid thermal response because of the satellite's small ratio of mass to area. The rapid thermal response characteristic makes it highly desirable to maintain the satellite in a continuous sunlight orbit since the inflation compounds become ineffective at the low shadow temperatures.

The maximum external deforming loads were found to result from incident solar radiation at altitudes above about 800 kilometers, whereas the aerodynamic forces are greatest below this altitude. The characteristic effect of the satellite's memory of its original folded condition is the major source of deforming loads for the Echo I satellite.

Micrometeoroids were estimated to produce holes with areas totaling about 28.1 square centimeters per day; these holes would permit the inflation vapors to leak out in approximately 13 days. In making this analysis, it was found that the influx of micrometeoroids may be somewhat higher, based on the referenced experimental data, than that previously predicted for some theoretical considerations.

Subliming organic compounds are commercially available that have vapor pressure characteristics that lend themselves very well to this application. By use of the proper amount of compound, good safety factors can be attained against rupturing the sphere as a result of overpressurizing due to overheating. Therefore, the performance of the inflation system in the static condition is nonsensitive to temperatures above that actually required, whereas the performance remains very sensitive to lower temperatures.

The weight of pressure-sustaining compounds would become prohibitive for long lifetime satellites subject to the predicted micrometeoroid puncturing although a subliming compound would be ideal as the initial inflation system where the sphericity could be preserved by mechanically, thermally, or chemically rigidification of the skin. The subliming compound for such applications would be required to maintain sphericity for only a short period of time necessary for the rigidification. The satellite would then no longer be dependent on internal pressure to maintain sphericity.

The compatibility of the subliming powders with necessary folding and packaging techniques is excellent. The powders can be distributed uniformly on the inside surface of the satellite and thus, are subject to immediate heating when released in orbit; as a result, increasing vapor pressure is

provided for inflation. This method of inflation requires no weight consumption for gas-storage bottles, no gas-injection mechanism, and is very simple and reliable.

Langley Research Center,
National Aeronautics and Space Administration,
Langley Station, Hampton, Va., December 12, 1963.

APPENDIX A

THERMAL RESPONSE OF A SPHERICAL SATELLITE ENTERING AND LEAVING SHADOW OF EARTH

The general equation for radiation heat transfer is

$$mc_p \frac{d\overline{T}}{dt} = \left(\frac{dq}{dt}\right)_S + \left(\frac{dq}{dt}\right)_R + \left(\frac{dq}{dt}\right)_E - \left(\frac{dq}{dt}\right)_B \tag{A1}$$

The first case considered is for the condition when the satellite enters the earth's shadow. The first two terms on the right-hand side of equation (A1) are zero in the shadow; therefore,

$$mc_p \frac{d\overline{T}}{dt} = \left(\frac{dq}{dt}\right)_E - \left(\frac{dq}{dt}\right)_B \tag{A2}$$

where

$$\left(\frac{dq}{dt}\right)_E = \pi R_B{}^2 C_S \alpha_E \frac{1 - a}{2}\left[1 - \left(1 - k^2\right)^{1/2}\right] \tag{A3}$$

and

$$\left(\frac{dq}{dt}\right)_B = 4\pi R_B{}^2 \epsilon_o \sigma \overline{T}^4 \tag{A4}$$

Substituting equations (A3) and (A4) into equation (A2) gives

$$\frac{d\overline{T}}{dt} = \frac{\pi R_B{}^2 C_S \alpha_E \left(\frac{1 - a}{2}\right)\left[1 - \left(1 - k^2\right)^{1/2}\right] - 4\pi R_B{}^2 \epsilon_o \sigma \overline{T}^4}{mc_p} \tag{A5}$$

Let

$$w^2 = \frac{\pi R_B{}^2 C_S \alpha_E}{m}\left(\frac{1 - a}{2}\right)\left[1 - \left(1 - k^2\right)^{1/2}\right]$$

$$x^2 = \frac{4\pi R_B{}^2 \epsilon_o \sigma}{m}$$

$$y^2 + z^2\overline{T} = c_p$$

Then

$$\frac{d\overline{T}}{dt} = \frac{w^2 - x^2\overline{T}^4}{y^2 + z^2\overline{T}} \tag{A6}$$

Equation (A6) can now be expanded for integration to

$$y^2 \int_{\overline{T}_o}^{\overline{T}} \frac{d\overline{T}}{w^2 - x^2\overline{T}^4} + z^2 \int_{\overline{T}_o}^{\overline{T}} \frac{\overline{T}\, d\overline{T}}{w^2 - x^2\overline{T}^4} = \int_{t_o}^{t} dt \tag{A7}$$

where $\overline{T}_o$ is the satellite temperature as it enters the earth's shadow at time $t_o = 0$.

The first term in equation (A7) can be integrated by the method of partial fractions to obtain

$$y^2 \int_{\overline{T}_o}^{\overline{T}} \frac{d\overline{T}}{w^2 - x^2\overline{T}^4} = \frac{y^2}{2wx\sqrt{\frac{w}{x}}}\left(\tan^{-1} \frac{\overline{T}}{\sqrt{\frac{w}{x}}} - \frac{1}{2} \log_e \frac{\overline{T} - \sqrt{\frac{w}{x}}}{\overline{T} + \sqrt{\frac{w}{x}}}\right)\Bigg]_{\overline{T}_o}^{\overline{T}} \tag{A8}$$

The second term in equation (A7) can be arranged in the form

$$\frac{z^2}{x^2} \int_{\overline{T}_o}^{\overline{T}} \frac{\overline{T}\, d\overline{T}}{\frac{w^2}{x^2} - \overline{T}^4} \tag{A9}$$

and integrated to give

$$\frac{z^2}{x^2} \int_{\overline{T}_o}^{\overline{T}} \frac{\overline{T}\, d\overline{T}}{\frac{w^2}{x^2} - \overline{T}^4} = -\frac{z^2}{4wx}\left(\log_e \frac{\overline{T}^2 - \frac{w}{x}}{\overline{T}^2 + \frac{w}{x}}\right)\Bigg]_{\overline{T}_o}^{\overline{T}} \tag{A10}$$

Equation (A7) can now be expressed as the sum of equations (A8) and (A10) giving

$$t_{sh} = \frac{y^2}{2wx\sqrt{\frac{w}{x}}}\left(\tan^{-1}\frac{\overline{T}}{\sqrt{\frac{w}{x}}} - \frac{1}{2}\log_e\frac{\overline{T} - \sqrt{\frac{w}{x}}}{\overline{T} + \sqrt{\frac{w}{x}}}\right)\Bigg]_{\overline{T}_o}^{\overline{T}} - \frac{z^2}{4wx}\log_e\left(\frac{\overline{T}^2 - \frac{w}{x}}{\overline{T}^2 + \frac{w}{x}}\right)\Bigg]_{\overline{T}_o}^{\overline{T}} \tag{A11}$$

where the equation must be evaluated over the interval $\overline{T}_o$ to $\overline{T}$ as indicated, and t_{sh} is the time required for the satellite temperature to decrease from $\overline{T}_o$ to $\overline{T}$.

The second case considered is for the conditions when the satellite leaves the earth's shadow. In this case

$$\left(\frac{dq}{dt}\right)_S = \pi R_B{}^2 C_S \alpha_S \tag{A12}$$

and

$$\left(\frac{dq}{dt}\right)_R = \pi R_B{}^2 C_S \alpha_S a2\left[1 - \left(1 - k^2\right)^{1/2}\right] \tag{A13}$$

and the parameters describing the rate of thermal energy absorbed directly from the earth and the rate that heat is radiated from the satellite are the same as in the first case. Substituting equations (A3), (A4), (A12), and (A13) into equation (A1) gives

$$\frac{d\overline{T}}{dt} = \frac{\pi R_B{}^2 C_S \alpha_S \left\{1 + \left[2aF_R(\beta) + \frac{\alpha_E}{\alpha_S}\frac{1 - a}{2}\right]\left[1 - \left(1 - k^2\right)^{1/2}\right]\right\} - 4\pi R_B{}^2 \epsilon_o \sigma \overline{T}^4}{mc_p} \tag{A14}$$

It is seen that this equation has the same form as equation (A5) where only the rate of radiation received by the satellite has changed from that described by w^2 in the first case to the present rate described by

$$w_1{}^2 = \frac{\pi R_B{}^2 C_S \alpha_S}{m}\left\{1 + \left[2aF_R(\beta) + \frac{\alpha_E}{\alpha_S}\frac{1 - a}{2}\right]\left[1 - \left(1 - k^2\right)^{1/2}\right]\right\} \tag{A15}$$

Equation (A14) is readily integrated by the same method used in the first case giving

$$t_{su} = \frac{y^2}{2w_1x\sqrt{\frac{w_1}{x}}}\left(\tan^{-1}\frac{\overline{T}}{\sqrt{\frac{w_1}{x}}} + \frac{1}{2}\log_e\frac{\sqrt{\frac{w_1}{x}} + \overline{T}}{\sqrt{\frac{w_1}{x}} - \overline{T}}\right)\Bigg]_{\overline{T}_o}^{\overline{T}} + \frac{z^2}{4w_1x}\left(\log_e\frac{\frac{w_1}{x} + \overline{T}^2}{\frac{w_1}{x} - \overline{T}^2}\right)\Bigg]_{\overline{T}_o}^{\overline{T}} \qquad \text{(A16)}$$

where $\overline{T}_o$ is the satellite temperature as it emerges from the earth's shadow into sunlight and $\overline{T}$ is the temperature at any time t_{su} after leaving the shadow.

APPENDIX B

CALCULATION OF PRESSURE TIME HISTORY INSIDE A VESSEL

The mass flow equation for free molecular flow (ref. 15) is

$$\frac{-dm}{dt} = 4.375 \times 10^{-5} p \sqrt{\frac{M}{T}} A \tag{B1}$$

From the kinetic theory of gases, it is known that

$$m = \frac{NM}{N_g} \tag{B2}$$

Substituting equation (B2) into equation (B1) gives

$$\frac{-dN}{dt} = 4.375 \times 10^{-5} \frac{N_g}{M} p \sqrt{\frac{M}{T}} A \tag{B3}$$

From the kinetic theory of gases, it is also known that

$$pV = N \frac{R_g}{N_g} T \tag{B4}$$

Now, substituting equation (B4) into equation (B3) for N the results are

$$\frac{-dp}{p} = 4.375 \times 10^{-5} R_g \sqrt{\frac{T}{MV^2}} A \, dt \tag{B5}$$

Substituting for R_g in equation (B5) and integrating gives

$$p = \frac{p_o}{\exp\left(C' \int_{t_o}^{t} A \, dt\right)} \tag{B6}$$

where

$$C' = 3.6378 \times 10^3 \sqrt{\frac{T}{MV^2}} \tag{B7}$$

When the leakage area in the wall of the vessel consists of both fixed holes and those that change with time, an expression for the total hole area at any time t is

$$A = f + gt \tag{B8}$$

Substituting equation (B8) into equation (B6) and integrating gives

$$p = \frac{p_o}{\exp\left[C'\left(f + \frac{1}{2}gt^2\right)\right]} \tag{B9}$$

REFERENCES

1. Cuddihy, William F., and Shreve, Lloyd H.: Microwave Reflectivity of Deposited Aluminum Films for Passive Relay Communications. NASA TN D-664, 1961.

2. Wood, George P., and Carter, Arlen F.: Predicted Characteristics of an Inflatable Aluminized-Plastic Spherical Earth Satellite With Regard to Temperature, Visibility, Reflection of Radar Waves, and Protection From Ultraviolet Radiation. NASA TN D-115, 1959.

3. Ballinger, J. C., Elizalde, J. C., and Christensen, E. H.: Thermal Environment of Interplanetary Space. [Preprint] 344B, Soc. Automotive Eng., 1961.

4. Manring, E., and Dubin, M.: Satellite Micrometeorite Measurements. IGY Satellite Series No. 3, IGY World Data Center A, Rockets and Satellites, National Academy of Sciences, May 1, 1958, pp. 25-30.

5. Whipple, Fred L.: The Meteoritic Risk to Space Vehicles. Proc. VIIIth International Astronautical Congress (Barcelona), F. Hecht, ed., Springer-Verlag (Vienna), 1958, pp. 418-428.

6. LaGow, H. E., and Alexander, W. M.: Recent Direct Measurements by Satellites of Cosmic Dust in the Vicinity of the Earth. NASA TN D-488, 1960.

7. Komissarov, O. D., Nazarova, T. N., Neugodov, L. N., Poloskov, S. M., and Rusakov, L. Z.: Investiation of Micrometeorites With Rockets and Satellites. Astronautics Information Translation No. 2 (Contract No. NASw-6), Jet Propulsion Lab., C.I.T., Sept. 4, 1959, pp. 99-108.

8. Dubin, M.: Meteoritic Dust Measured from Explorer I. Planetary and Space Sci., vol. 2, no. 2/3, Pergamon Press, Apr. 1960, pp. 121-129.

9. Watson, Fletcher G.: Between the Planets. Rev. ed., Harvard Univ. Press (Cambridge, Mass.), 1956.

10. Minzner, R. A., Champion, K. S. W., and Pond, H. L.: The ARDC Model Atmosphere, 1959. Air Force Surveys in Geophysics No. 115 (AFCRC-TR-59-267), Air Force Cambridge Res. Center, Aug. 1959.

11. Joos, George: Theoretical Physics. Second ed., Hafner Pub. Co., Inc. (New York), 1950.

12. Amborski, Leonard E., and Flierl, Donald W.: Physical Properties of Polyethylene Terephthalate Films. Ind. and Eng. Chem., vol. 45, no. 10, Oct. 1953, pp. 2290-2295.

13. Von Karman, Th., and Tsien, Hsue-Shen: The Buckling of Spherical Shells by External Pressure. Jour. Aero. Sci., vol. 7, no. 2, Dec. 1939, pp. 43-50.

14. Adamson, Arthur W.: Physical Chemistry of Surfaces. Interscience Publ., Inc. (New York), c.1960.

15. Dushman, Saul: Scientific Foundations of Vacuum Technique. John Wiley & Sons, Inc., c.1949.

16. Jensen, Niels: Vapor Pressure of Plastic Materials. Jour. Appl. Phys., vol. 27, no. 12, Dec. 1956, pp. 1460-1462.

17. Anon.: Interim Summary Report Investigation of a 15-KW Solar Dynamic Power System for Space Application. Tech. Doc. Rep. No. ASD-TDR-62-1002 (Contract No. AF33(616)-7128), Wright-Patterson Air Force Base, 1962.

18. Hougen, Olaf A., Watson, Kenneth M., and Ragatz, Roland A.: Chemical Process Principles. Part I - Material and Energy Balances. Second ed., John Wiley & Sons, Inc., c.1954.

19. Anderson, A. A., Jr., and Morfitt, G. L.: Balloon Barrier Materials. Rep. No. 1914 (AFCRC-TR-60-204), General Mills, Inc., Nov. 30, 1959.

20. Jakes, William C., Jr.: Participation of Bell Telephone Laboratories in Project Echo and Experimental Results. NASA TN D-1127, 1961.

21. Stull, Daniel R.: Vapor Pressure of Pure Organic Substances - Organic Compounds. Industrial and Engineering Chemistry, vol. 39, no. 4, April 1947, pp. 517-540.

22. Hoyer, H., and Peperle, W.: Dampfdruckmessungen an Organischen Substanzen und ihre Sublimationswärmen Zeitschrift für Elektrochemie, Bd. 62, Nr. 1, 1958.

TABLE I.- DATA CONCERNING THE HOLE-PRODUCING PROBABILITY OF MICROMETEOROIDS IN THE ECHO I SATELLITE

① Visual magnitude	② Mass, gm	③ Particle radius, cm	④ Particle cross section, cm^2	⑤ Number earth per m^2 per sec	⑥ Number Echo I per sec	⑦ Number Echo I per sec per visual magnitude	⑧ Holes Echo I per sec, cm^2
0	25	1.4254	6.383	3.048×10^{-14}	4.446×10^{-11}	5.229×10^{-11}	3.338×10^{-10}
1	9.95	1.0484	3.453	8.291×10^{-14}	1.209×10^{-10}	1.422×10^{-10}	4.915×10^{-10}
2	3.96	7.7125×10^{-1}	1.869	2.255×10^{-13}	3.289×10^{-10}	3.869×10^{-10}	7.231×10^{-10}
3	1.58	5.6778×10^{-1}	1.013	6.134×10^{-13}	8.947×10^{-10}	1.052×10^{-9}	1.066×10^{-9}
4	6.28×10^{-1}	4.1746×10^{-1}	5.474×10^{-1}	1.668×10^{-12}	2.433×10^{-9}	2.862×10^{-9}	1.567×10^{-9}
5	2.50×10^{-1}	3.0709×10^{-1}	2.963×10^{-1}	4.538×10^{-12}	6.619×10^{-9}	7.786×10^{-9}	2.307×10^{-9}
6	9.95×10^{-2}	2.2589×10^{-1}	1.603×10^{-1}	1.234×10^{-11}	1.800×10^{-8}	2.118×10^{-8}	3.395×10^{-9}
7	3.96×10^{-2}	1.6616×10^{-1}	8.674×10^{-2}	3.358×10^{-11}	4.897×10^{-8}	5.760×10^{-8}	4.996×10^{-9}
8	1.58×10^{-2}	1.2239×10^{-1}	4.706×10^{-2}	9.132×10^{-11}	1.332×10^{-7}	1.567×10^{-7}	8.940×10^{-9}
9	6.28×10^{-3}	8.993×10^{-2}	2.541×10^{-2}	2.484×10^{-10}	3.623×10^{-7}	4.262×10^{-7}	1.083×10^{-8}
10	2.50×10^{-3}	6.616×10^{-2}	1.375×10^{-2}	6.757×10^{-10}	9.855×10^{-7}	1.159×10^{-6}	1.594×10^{-8}
11	9.95×10^{-4}	4.866×10^{-2}	7.438×10^{-3}	1.838×10^{-9}	2.681×10^{-6}	3.153×10^{-6}	2.345×10^{-8}
12	3.96×10^{-4}	3.580×10^{-2}	4.026×10^{-3}	4.999×10^{-9}	7.291×10^{-6}	8.575×10^{-6}	3.453×10^{-8}
13	1.58×10^{-4}	2.636×10^{-2}	2.183×10^{-3}	1.360×10^{-8}	1.983×10^{-5}	2.333×10^{-5}	5.092×10^{-8}
14	6.28×10^{-5}	1.937×10^{-2}	1.179×10^{-3}	3.698×10^{-8}	5.395×10^{-5}	6.345×10^{-5}	7.481×10^{-8}
15	2.50×10^{-5}	1.425×10^{-2}	6.379×10^{-4}	1.006×10^{-7}	1.467×10^{-4}	1.726×10^{-4}	1.101×10^{-7}
16	9.95×10^{-6}	1.049×10^{-2}	3.457×10^{-4}	2.736×10^{-7}	3.991×10^{-4}	4.694×10^{-4}	1.623×10^{-7}
17	3.96×10^{-6}	7.71×10^{-3}	1.867×10^{-4}	7.443×10^{-7}	1.086×10^{-3}	1.277×10^{-3}	2.384×10^{-7}
18	1.58×10^{-6}	5.68×10^{-3}	1.014×10^{-4}	2.024×10^{-6}	2.953×10^{-3}	3.473×10^{-3}	3.522×10^{-7}
19	6.28×10^{-7}	4.17×10^{-3}	5.463×10^{-5}	5.506×10^{-6}	8.032×10^{-3}	9.446×10^{-3}	5.160×10^{-7}
20	2.50×10^{-7}	3.07×10^{-3}	2.961×10^{-5}	1.498×10^{-5}	2.185×10^{-2}	2.572×10^{-2}	7.615×10^{-7}
21	9.95×10^{-8}	2.26×10^{-3}	1.605×10^{-5}	4.074×10^{-5}	5.942×10^{-2}	6.989×10^{-2}	1.122×10^{-6}
22	3.96×10^{-8}	1.66×10^{-3}	8.657×10^{-6}	1.108×10^{-4}	1.616×10^{-1}	1.895×10^{-1}	1.639×10^{-6}
23	1.58×10^{-8}	1.224×10^{-3}	4.707×10^{-6}	3.014×10^{-4}	4.396×10^{-1}	5.172×10^{-1}	2.437×10^{-6}
24	6.28×10^{-9}	8.99×10^{-4}	2.539×10^{-6}	8.198×10^{-4}	1.196×10^{0}	1.406×10^{0}	3.571×10^{-6}
25	2.50×10^{-9}	6.62×10^{-4}	1.377×10^{-6}	2.230×10^{-3}	3.253×10^{0}	3.826×10^{0}	5.268×10^{-6}
26	9.95×10^{-10}	4.87×10^{-4}	7.451×10^{-7}	6.066×10^{-3}	8.847×10^{0}	1.040×10^{1}	7.752×10^{-6}
27	3.96×10^{-10}	3.62×10^{-4}	4.117×10^{-7}	1.650×10^{-2}	2.406×10^{1}	2.830×10^{1}	1.165×10^{-5}
28	1.58×10^{-10}	2.64×10^{-4}	2.189×10^{-7}	4.487×10^{-2}	6.545×10^{1}	7.698×10^{1}	1.685×10^{-5}
29	6.28×10^{-11}	1.94×10^{-4}	1.182×10^{-7}	1.221×10^{-1}	1.780×10^{2}	2.094×10^{2}	2.475×10^{-5}
30	2.50×10^{-11}	1.43×10^{-4}	6.424×10^{-8}	3.320×10^{-1}	4.843×10^{2}	5.696×10^{2}	3.659×10^{-5}
31	9.95×10^{-12}	1.00×10^{-4}	3.142×10^{-8}	9.030×10^{-1}	1.317×10^{3}	1.549×10^{3}	4.868×10^{-5}

TABLE II.- PHYSICAL PROPERTIES OF SOME ORGANIC SUBLIMING COMPOUNDS

Compound	Formula	Molecular weight	Density, gram/cm^3	Melting point, °C	Boiling point, °C	Subliming properties		Temperature interval of measurements, °C	Reference
						Heat of sublimation, ergs/gm-mole	Vapor pressure, $\log_e p = A' - \frac{B'}{T}$		
d-Camphor	$C_{10}H_{16}O$	152.23	1.000	178.5	204	5.073×10^{11}	$26.571 - \frac{6090}{T}$	40 to 210	21
Naphthalene	$C_{10}H_8$	128.16	1.145	80.22	217.9	6.739×10^{11}	$31.948 - \frac{8326}{T}$	-20 to 10	22
Benzoic acid	$C_7H_6O_2$	122.12	1.2659	121.7	249	6.848×10^{11}	$29.595 - \frac{8223}{T}$	96 to 250	21
Anthracene	$C_{14}H_{10}$	178.22	1.25	217	354	10.339×10^{11}	$36.530 - \frac{12436}{T}$	30 to 100	22
Anthraquinone	$C_{14}H_8O_2$	208.20	1.419	286	379	12.307×10^{11}	$40.145 - \frac{15206}{T}$	70 to 130	22